**AGU100** ADVANCING EARTH AND SPACE SCIENCE

# Mesozoic Development of Nonmarine Basins in the Northern Yidun Terrane: Deposition and Deformation in the Eastern Tibetan Plateau Prior to the India-Asia Collision

W. T. Jackson Jr.[1,2] (ID), D. M. Robinson[2], A. L. Weislogel[3], F. Shang[4], and X. Jian[5]

[1]Department of Earth Sciences, University of South Alabama, Mobile, AL, USA, [2]Department of Geological Sciences and Center for Sedimentary Basin Studies, The University of Alabama, Tuscaloosa, AL, USA, [3]Department of Geography and Geology, West Virginia University, Morgantown, WV, USA, [4]Research Institution of Petroleum Exploration and Development, PetroChina, Beijing, China, [5]College of Ocean and Earth Sciences, Xiamen University, Xiamen, China

**Abstract** To determine the timing and spatial patterns of syntectonic nonmarine deposition and deformation in the eastern Tibetan Plateau, we present field data, thin section petrology, and detrital U-Pb zircon geochronology from the west Ganzi basin (WGB) and east Ganzi basin (EGB) in the northern Yidun terrane. The WGB and EGB contain ~800 and ~1,300–1,600 m of nonmarine strata, respectively, deposited in alluvial environments. Along the southern margins of both the WGB and EGB and the northwestern margin of the WGB, reverse faults place Triassic Ganzi Pluton and Triassic Yidun Grouprocks on top of nonmarine strata. Growth strata in the footwalls of basin-bounding faults indicate that deposition was synchronous with fault development. The western and eastern margins of the WGB, as well as the northern margin of the EGB, exhibit uncomformable contacts with the underlying Triassic Ganzi Pluton and Triassic Yidun Grouprocks. Provenance results suggest a regionally mixed sediment source from the Yidun and Songpan-Ganzi terranes. Maximum deposition ages from detrital U-Pb zircon geochronology, as well as previously reported thermochronology and palynology results, indicate a Late Mesozoic depositional age for WGB and EGB strata. We interpret the spatial and temporal developments of the WGB and EGB to be associated with the Lhasa-Qiangtang collision.

## 1. Introduction

Despite the ever-growing documentation for the tectonic evolution of the southern margin of Eurasia prior to the India-Asia collision, spatial and temporal patterns of Mesozoic deformation remain unclear throughout the eastern Tibetan Plateau (Burchfiel & Chen, 2012). Mesozoic tectonism throughout the Tibetan Plateau controlled the development of the lithospheric architecture that was later modified by the development of the Cenozoic Himalaya-Tibetan orogenic system (Burchfiel & Chen, 2012; Dewey et al., 1988; Horton et al., 2002; Metcalfe, 1996; Yin & Harrison, 2000). In the eastern Tibetan Plateau, widespread Triassic deformation associated with collisional tectonism and closure of the Paleo-Tethys Ocean (Harrowfield & Wilson, 2005; Pullen et al., 2008; Reid et al., 2005; Roger et al., 2004, 2010; Weislogel, 2008) is recorded by turbidite deposition and deformation in the Songpan-Ganzi and Yidun terranes, as well as pluton development associated with subduction along the Ganzi-Litang suture (Reid et al., 2005, 2007; Roger et al., 2010; Wang, Zhou, et al., 2013; Weislogel, 2008; Zhou & Graham, 1996). Post-Triassic deformational phases associated with the Lhasa-Qiangtang collision during Middle Cretaceous time and the northward oceanic subduction of the Indian plate in Late Cretaceous-early Cenozoic time along the southern margin of Eurasia further deformed Mesozoic rocks, resulting in an Andean-like margin (Guynn et al., 2006; DeCelles et al., 2007; Kapp et al., 2003, 2007; Murphy et al., 1997).

To reconstruct the Mesozoic development of the Tibetan Plateau, stratigraphic chronologies from Mesozoic sedimentary basins throughout the plateau are required (Horton et al., 2002; Yin & Harrison, 2000). Post-Triassic strata in the interior of the eastern Tibetan Plateau are primarily composed of oxidized nonmarine sedimentary rock, which in most cases lack diagnostic fossils, datable volcanic layers/intrusions, and regional lithostratigraphic correlations (DeCelles et al., 2007; Horton et al., 2002, 2004; Kidd et al., 1988; Wang et al., 2001; Yin et al., 1988). Along with these complications, the multiple episodes of deformation exacerbate the difficulty in assigning ages to these sedimentary strata (e.g., Craddock et al., 2012; Kapp et al., 2007; Spurlin et al., 2005; Studnicki-Gizbert et al., 2008). Located in the eastern Tibetan Plateau, the Yidun terrane hosts nonmarine basins previously assigned Cenozoic ages during regional surveying (Bureau of Geology
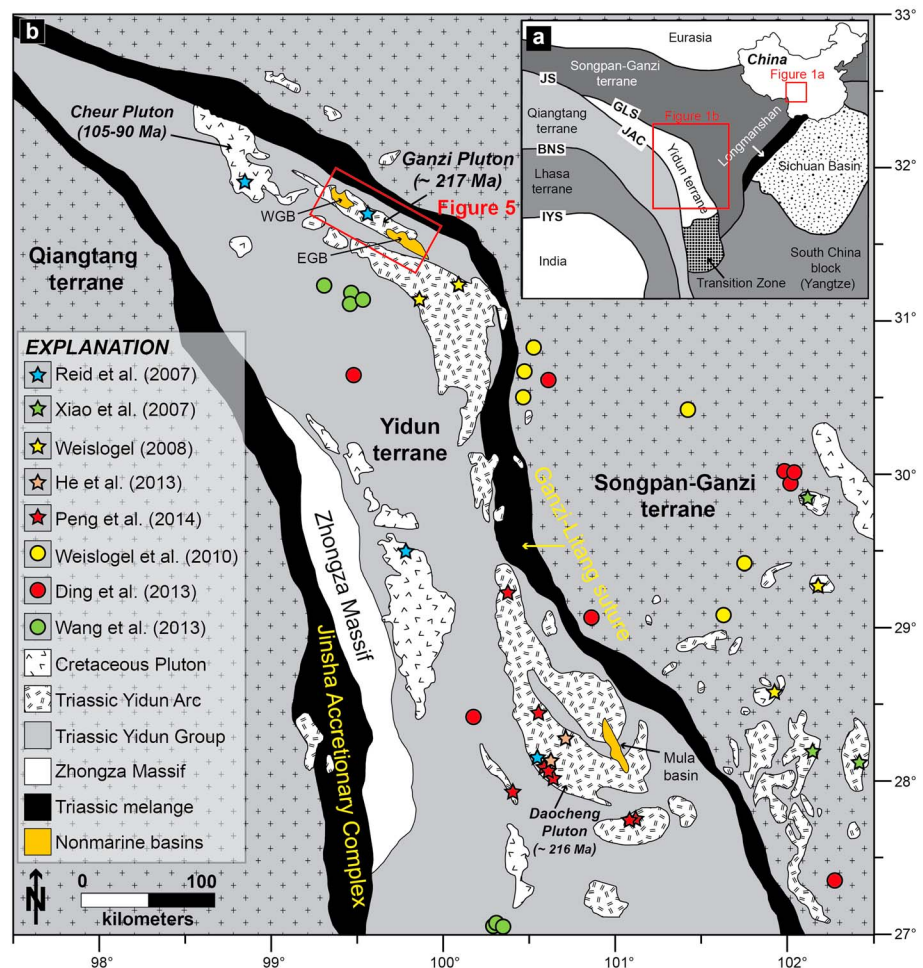
**Figure 1.** (a) Regional tectonic map for the eastern Tibetan Plateau. Insert illustrates the location of Figure 2a relative to China. Major suture zones are delineated on map of China. GLS = Ganzi-Litang suture, JAC = Jinsha Accretionary Complex, JS = Jinsha suture, BNS = Bangong-Nijiang suture, IYS = Indus-Yarlong suture. (b) Generalized geologic map for the Yidun terrane, with location of the west Ganzi basin and east Ganzi basin. Colored circles indicate location of previously published detrital zircon geochronology. Colored stars indicate location of previously published geochronology of plutonic bodies. Base map adapted from Bureau of Geology and Mineral Resources of Sichuan Province (1991), Burchfiel and Chen (2012), and Wang, Wang, Chen, et al. (2013).

and Mineral Resources of Sichuan Province, 1991). However, a Cenozoic age for all nonmarine basins in the Yidun terrane is questionable as previously reported palynology results suggest that nonmarine strata in the northern Yidun terrane exhibit Cretaceous depositional ages (Liu, 1999).

The purpose of this study is to document sedimentological and structural data from two nonmarine basins in the northern part of the Yidun terrane, the west Ganzi basin (WGB) and east Ganzi basin (EGB; Figure 1, Figure 2). This work contributes toward an assessment of nonmarine deposition and deformation in the eastern Tibetan Plateau, as well as a better understanding of the influence of inherited Mesozoic tectonics on Cenozoic deformation associated with the India-Asia collision. We present field measurements, detrital U-Pb zircon geochronology, and thin section petrology to address the tectonic setting, stratigraphic age, and sedimentary provenance of the WGB and EGB basin fill.

## 2. Geologic Setting

### 2.1. Eastern Tibetan Plateau

The eastern Tibetan Plateau consists of multiple terranes that are separated by Paleo- and Meso-Tethys ocean sutures. These terranes contain a record of Paleozoic through early Mesozoic rifting followed by Mesozoic
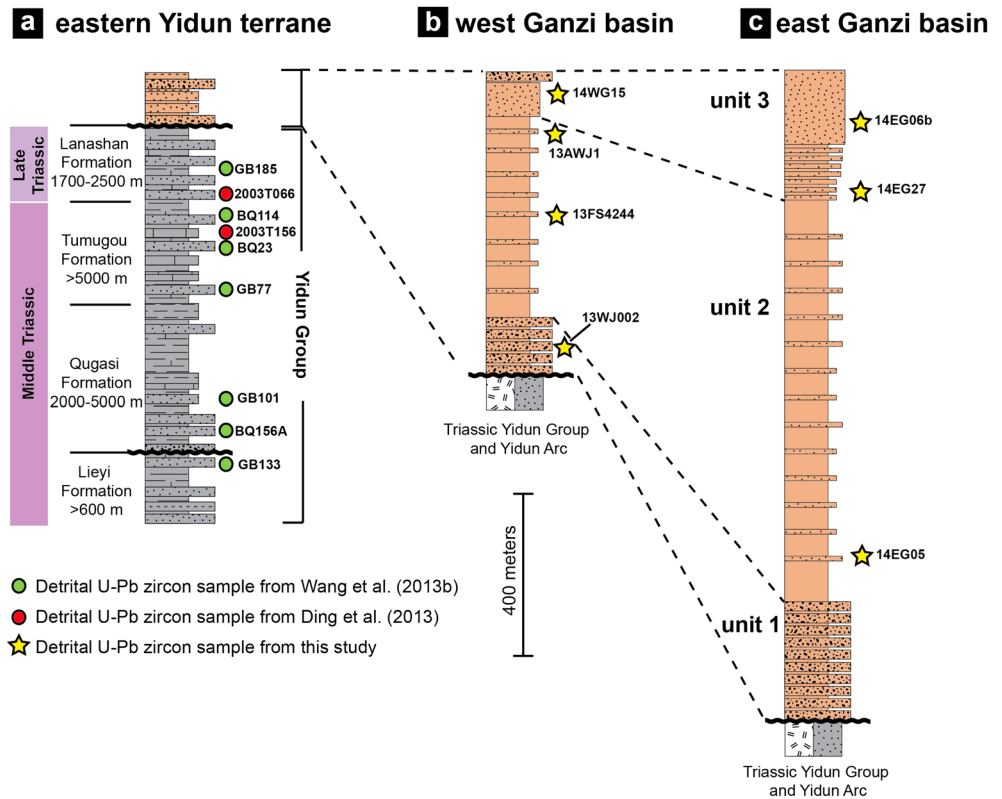
**Figure 2.** Stratigraphic columns and correlation for (a) the eastern Yidun terrane, (b) west Ganzi basin, and (c) east Ganzi basin. Stratigraphic positions and sample number are shown for detrital zircon samples in the Yidun Group by Wang, Wang, Chen, et al. (2013) and Ding et al. (2013) and the west Ganzi basin and east Ganzi basin samples from this study. Units 1, 2, and 3 are correlated in (b) and (c). Scale bar is only for (b) and (c).

amalgamation to the southern margin of Eurasia (Burchfiel & Chen, 2012; Dewey et al., 1988; Yin & Harrison, 2000). Following Mesozoic collisions, India collided with southern Eurasia in early Cenozoic time (DeCelles et al., 2014; Hu et al., 2016; Leech et al., 2005; Lippert et al., 2014; Najman et al., 2010; Orme et al., 2015; Wang et al., 2011). Cenozoic deformation in response to India-Asia collision is marked by contractional structures and nonmarine deposition throughout the plateau (Kapp et al., 2007; Yin & Harrison, 2000). In the eastern Tibetan Plateau, during early Cenozoic time, contractional upper-crustal shortening persisted in conjunction with the initiation of southeastward extrusion of crustal blocks that was initiated in response to continental collision (Burchfiel et al., 1995; Tapponnier et al., 1982; 2001; Wang & Burchfiel, 1997). During late Miocene time, strike-slip deformation became the prominent stress regime and further propagated extrusion of crustal material to the southeast (Clark et al., 2005; Royden et al., 2008).

### 2.2. Yidun Terrane

The Yidun terrane is positioned between the Qiangtang terrane to the west and the Songpan-Ganzi terrane to the east and north and is bounded by two Paleo-Tethys suture zones. The Jinsha Accretionary Complex, also referred to as the Jinsha-Jiang suture, separates the Qiangtang terrane to the southwest from the Yidun terrane. The Jinsha Accretionary Complex developed during Early-Middle Triassic time in response to Zhongza Massif and Qiangtang terrane collision (Reid et al., 2005; Wang et al., 2000). The Ganzi-Litang suture separates the Songpan-Ganzi terrane to the north and northeast from the Yidun terrane. The Ganzi-Litang suture developed during Late Triassic time in response to westward subduction beneath the eastern Yidun terrane (Reid et al., 2007; Weislogel, 2008).

The Yidun terrane is separated into eastern and western regions. The western region, referred to as the Zhongza Massif, is characterized by a meta-sedimentary Paleozoic passive margin sequence (Chen & Chen, 1987). The eastern Yidun contains the Late Triassic Yidun Arc (Li et al., 2017; Reid et al., 2007; Weislogel, 2008) and Triassic Yidun Group turbidite rock (Wang, Zhou, et al., 2013; Wang, Wang, Chen, et al., 2013;

Wang, Wang, & Zhou, 2013). The Late Triassic Yidun Arc is a north-south trending, rhyolitic/calc-alkaline plutonic field along the eastern margin of the Yidun terrane, with ages ranging from ~225 to 215 Ma (He et al., 2013; Peng et al., 2014; Wu et al., 2016). Formation of the Yidun Arc may record subduction along the eastern Yidun terrane that produced the Ganzi-Litang suture in Late Triassic time (Chen & Chen, 1987; Leng et al., 2014; Wang et al., 2011). The Triassic Yidun Group is a ~5–12-km-thick turbidite and volcanic sedimentary sequence (Bureau of Geology and Mineral Resources of Sichuan Province, 1991; Hou, 1993; Wang, Wang, Chen, et al., 2013). Detrital U-Pb zircon studies on Triassic Yidun Group show age peaks at 220–240, 400–480, 720–880, 880–980, 1,790–1,900, and 2,450–2,500 Ma (Ding et al., 2013; Jian et al., 2015; Wang, Wang, Chen, et al., 2013). Wang, Wang, Chen, et al. (2013) illustrate that turbidite rocks from the northern and southern Yidun terrane exhibit different signatures for time equivalent strata, resulting from deposition in two different systems. Turbidite rocks in the northern Yidun terrane contain only two prominent age peaks, 400–480 and 880–980 Ma, with a third minor age peak at 2,450–2,500 Ma. Turbidite rocks in the southern Yidun terrane contain the three age peaks present in northern Yidun terrane, along with peaks at 220–240, 720–880, and 1,750–1,900 Ma. For the northern and southern Yidun Group, a Zhongza Massif provenance is inferred, with the southern Yidun Group also receiving material from the Triassic Yidun Arc represented by the 200–250 Ma zircon population (Ding et al., 2013; Wang, Wang, Chen, et al., 2013).

### 2.3. Nonmarine Strata

Nonmarine basins throughout the Tibetan Plateau contain a record of upper-crustal deposition and deformation associated with plateau growth resulting from the India-Asia collision (Yin & Harrison, 2000). These basins tend to be elongate in shape, located in the footwalls of thrust faults, and spatially near Mesozoic sutures (Studnicki-Gizbert et al., 2008). While precise dating of these basins is difficult (i.e., Horton et al., 2004), nonmarine strata throughout the plateau have predominantly been assigned Paleogene ages based on fossil assemblages, geochronology, and palynological data (Bureau of Geology and Mineral Resources of Sichuan Province, 1991; DeCelles et al., 2007; Liu et al., 2001; Rowley, 1996; Spurlin et al., 2005).

Throughout the eastern half of the Yidun terrane nonmarine basins are present and identified based on their red and maroon coloring (Bureau of Geology and Mineral Resources of Sichuan Province, 1991). These basins range from a few hundred meters to >2,000 m thick, are assigned Paleogene ages, and generally lie within the footwalls of thrust faults (Burchfiel & Chen, 2012). Jackson et al. (2018) show that nonmarine basin fill of the Mula basin, located in the southern Yidun terrane, exhibits a Cenozoic age, is deposited in alluvial environments, and is associated with contractional deformation associated with the India-Asia collision. Nonmarine strata in the WGB and EGB share similarities such as color and stratigraphic architecture with nonmarine strata in the Mula basin and other nonmarine deposits throughout the Tibetan Plateau (e.g., Horton et al., 2002; Wang et al., 2014). However, Liu (1999) suggests a Mesozoic age for the WGB based on palynology results.

### 2.4. Songpan-Ganzi Terrane

The Songpan-Ganzi terrane consists predominantly of a ~10–15-km-thick Middle to Late Triassic turbidite sequence that covers an area of >200,000 km$^2$ (Nie et al., 1994; Zhou & Graham, 1996). Turbidite rocks from the Songpan-Ganzi terrane are similar to Yidun Group turbidite rocks in hand specimen and thin section. Detrital U-Pb zircon results show that eastern Songpan-Ganzi turbidite strata formed in three distinct depocenters, sourced from North China, Qinling-Dabie, South China, and Yidun/Qiangtang terranes (Enkelmann et al., 2007; Weislogel et al., 2006, 2010). Studies conducted on Triassic Songpan-Ganzi terrane turbidites from the southeastern depocenter show age peaks that correspond to all the observed age peaks in the Yidun Group, with populations at 220–250, 400–500, 730–820, ~1,850, and ~2,400 Ma (Ding et al., 2013; Weislogel et al., 2006, 2010). Further detrital zircon and Hf isotopic work on the Songpan-Ganzi turbidites suggest that the southeastern depocenters of the Songpan-Ganzi terrane turbidites and Yidun Group turbidites were connected as a large regional depocenter during Late Triassic time (Ding et al., 2013; Jian et al., 2014, 2015; Weislogel et al., 2010).

## 3. Methods

### 3.1. Field Procedures

This study targeted nonmarine strata of the remote WGB and EGB. Most rocks crop out near the top of ridges ~300–500 m above the base elevation of ~3,800 m. Sampling distribution and density in the WGB and EGB

were controlled primarily by rock type (medium-grained sandstone to granule-conglomerate) and accessibility to outcrops. Fracture orientations were measured, along with abutting relationships to assess strain and structural reactivation. Nine conglomerate clast counts were collected to augment thin section petrology and detrital U-Pb zircon geochronology provenance data, and nine conglomerate clast counts were collected. For conglomerate clast counts, the rock types of 50–100 clasts were counted using a 2-cm spacing over a 1-m by 1-m grid. Rock descriptions, field measurements, and sample locations are in Table S1 in the supporting information.

### 3.2. Detrital U-Pb Zircon Geochronology

Seven samples were analyzed for detrital U-Pb zircon geochronology, four samples from the WGB and three samples from the EGB. Samples weighing 1 to 4 kg of medium-grained sandstone to granule conglomerate were collected. Zircons were separated, mounted, and imaged at the University of Alabama and University of Arizona following procedures outlined by Gehrels et al. (2006, 2008). Ages were collected with a Nu Plasma multi-collector LA-ICP-MS (samples 13AWJ1, 13FS4244, 13WJ002, 14EG06b, and 14EG27) and an Element2 single collector LA-ICP-MS (samples 14WG15 and 14EG05), both housed at the Arizona LaserChron Center. The acquisition routine on the multicollector followed that of Johnston et al. (2008), while the routine for the single collector followed steps outlined in Pullen et al. (2014). For a detailed description of the methodology, equipment, and performance of the LA-ICP-MS, refer to the University of Arizona's Laserchron Lab website (https://sites.google.com/a/laserchron.org/laserchron/). Zircon data reduction was processed using AgeCalc at the University of Arizona (Gehrels et al., 2008). Following data reduction, zircon ages were evaluated in two ways. For grains >900 Ma (based on $^{206}Pb/^{207}Pb$), ages were plotted on a Concordia diagram and evaluated based on 25% discordant or 5% reverse-discordant criteria. For grains <900 Ma (based on $^{206}Pb/^{238}U$), ages were plotted on a Concordia diagram for visual evaluation and filtered at 98% based on uranium abundance (ppm), thorium abundance (ppm), and initial lead concentration to remove any outliers. Results were analyzed and plotted using Isoplot 3.0 (Ludwig, 2012) and DensityPlotter (Vermeesch, 2012). Geochronology data are in Table S2.

The WGB and EGB did not contain volcanic ash layers, fossils, or dateable cross-cutting relationships to demonstrate stratigraphic age. In addition, while previously published palynology results from the WGB indicate a Cretaceous age (Liu, 1999), our samples selected for palynological analysis were barren. Therefore, detrital U-Pb zircon geochronology provides the best technique to determine nonmarine stratigraphic ages for these basins.

To determine the maximum depositional age (MDA) for each sample, a weighted mean average for the youngest detrital zircon age population was calculated (Dickinson & Gehrels, 2009a). Only using the youngest detrital zircon grain to determine the MDA may produce an age younger than the true depositional age (Dickinson & Gehrels, 2003, 2009b; Dehler et al., 2010). Because of the numerous geologic factors such as Pb loss and laboratory contamination that may affect the interpretation (Nelson, 2001; Sircombe, 1999), a weighted mean average of the youngest population with an *n*-value of ≥3 is required to ensure precision (Dickinson & Gehrels, 2009a; Vermeesch, 2004).

### 3.3. Thin Section Petrology

Nine thin sections were prepared for thin section petrology analysis and stained for potassium feldspar and calcic plagioclase identification. Four hundred framework grains were counted for each sample following the Gazzi-Dickinson method to minimize grain-size effects (Dickinson, 1970; Ingersoll et al., 1984). Results were plotted using a Microsoft Excel-based tool by Zahid and Barbeau (2011) on four ternary diagrams depicting provenance and tectonic relationships such as sediment maturity (total quartz-feldspar-lithics), source rock (monocrystalline quartz-feldspar-total lithics), feldspar fragments (monocrystalline quartz-plagioclase-potassium feldspar), and lithic fragments (polycrystalline quartz-volcanic lithics-sedimentary lithics; Dickinson, 1985; Dickinson & Suczek, 1979; Ingersoll, 1978). Petrology data are in Table S3.

## 4. Results

### 4.1. Stratigraphy

The WGB stratigraphy contains ~800 m of oxidized, red to purple strata (Figure 3). The basal unit, unit 1, is not well exposed. Where present, unit 1 is characterized by interbedded clast-supported pebble conglomerate (5–10 m thick) and mudstone/siltstone layers, for a total thickness of ~200 m (Figure 4). Stratigraphically
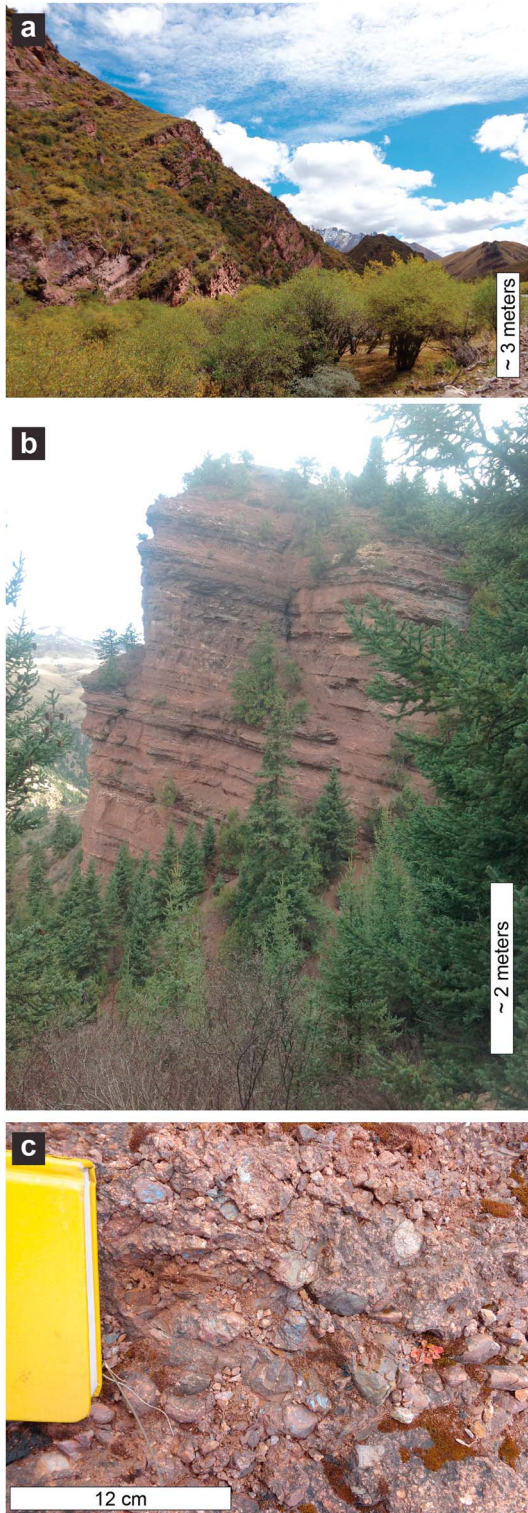
**Figure 3.** Field photographs from the west Ganzi basin (WGB) and east Ganzi basin (EGB) illustrating examples of unit 1, 2, and 3 stratigraphic intervals. (a) Dipping interbedded conglomerate, mudstone, and sandstone in the WGB representative of unit 1 strata. (b) Interbedded sandstone and mudstone indicative in the EGB representative of unit 2 strata. (c) Clast-supported conglomerate in the WGB representative of conglomerate in unit 1. Field book used for scale determination.

above unit 1, unit 2 consists of a ~400-m-thick sequence of mudstone, interbedded with fine- to medium-grained sandstone. Sandstone beds are medium-bedded, locally contain cross bedding, and are laterally continuous. Stratigraphically above unit 2, unit 3 exhibits ~200 m of predominantly fine- to medium-grained sandstone interbedded with thin (<1-m-thick) mudstone beds, capped by a 5-m-thick clast-supported pebble conglomerate.

The EGB stratigraphy contains ~1,300–1,600 m of oxidized white to red-purple strata (Figure 3). The basal unit, unit 1, varies from the western part to the eastern part of the basin, containing a total thickness of ~500–800 m. Throughout the western part of the EGB, unit 1 consists of 3–8-m-thick granule-pebble conglomerate beds interbedded with mudstone/siltstone and sandstone, while in the eastern part of the EGB, unit 1 consists of a 30–50-m-thick conglomerate, overlain by interbedded 10-cm- to 2-m-thick granule conglomerate and sandstone beds with increasing number of mudstone beds and mudstone bed thicknesses upsection. Stratigraphically above unit 1, unit 2 consists of ~500 m of mudstone/siltstone interbedded with 1–5-m-thick beds of fine- to medium-grained sandstone (Figure 4). Stratigraphically above unit 2, unit 3 is a coarsening-upward sequence of interbedded mudstone/siltstone and sandstone for ~100 m, with ~200 m of fine- to medium-grained sandstone upsection.

Conglomerate beds within the WGB and EGB are clast-supported and commonly exhibit crude horizontal planar stratification and imbrication, with rare long-angle planar cross bedding (Figure 4). Matrix consists of fine-grained sand to granule; however, in some places in unit 1, the matrix consists of orange, moderately well-sorted very fine to medium-grained sand. Conglomerate clast sizes range from 2 to 20 cm, with an average size of ~4 cm. Cobble-sized clasts are typically very angular to subangular, whereas pebble-sized clasts are typically subrounded to rounded. Clasts consistently exhibit indentations and ridges. Identified clast lithologies include red sandstone, red siltstone, red shale, white sandstone, tan/lithic sandstone, dark-gray to black shale/slate, granite, phyllite, vein quartz, and quartzite (Figure 5).

### 4.2. Basin Boundaries and Structure

Basin boundaries for the WGB and EGB exhibit either a fault or an unconformable contact with Triassic turbidite rocks and Triassic Ganzi Pluton (Yidun Arc; Figures 6 and 7). The WGB northern boundary is an ENE-WSW-oriented reverse fault that dips 55°NNW that curves away from the basin near both fault tips at the NW and NE ends (Figure 6). The fault places deformed Triassic Yidun Group turbidite rocks in the hanging wall over granite of the Ganzi Pluton and nonmarine growth strata in the footwall (Figures 7a and 7b). The WGB southern boundary is an ESE-WNW-oriented reverse fault that dips 60°SW, which places deformed Triassic Yidun Group turbidite rocks in the hanging wall over granite of the Ganzi Pluton and nonmarine growth strata in the footwall. Bedding dips of the growth strata systematically decrease upsection and basinward from ~75° to 90° adjacent to the fault to nearly horizontal ~20–25 m away from the bounding fault. This progressive decrease in bedding dip and the decrease in bed thickness toward the fault indicate synchronous fault slip and progressive bed tilting with sedimentation, which was greatest during early stages of basin deposition and decreased with time. Growth strata contain
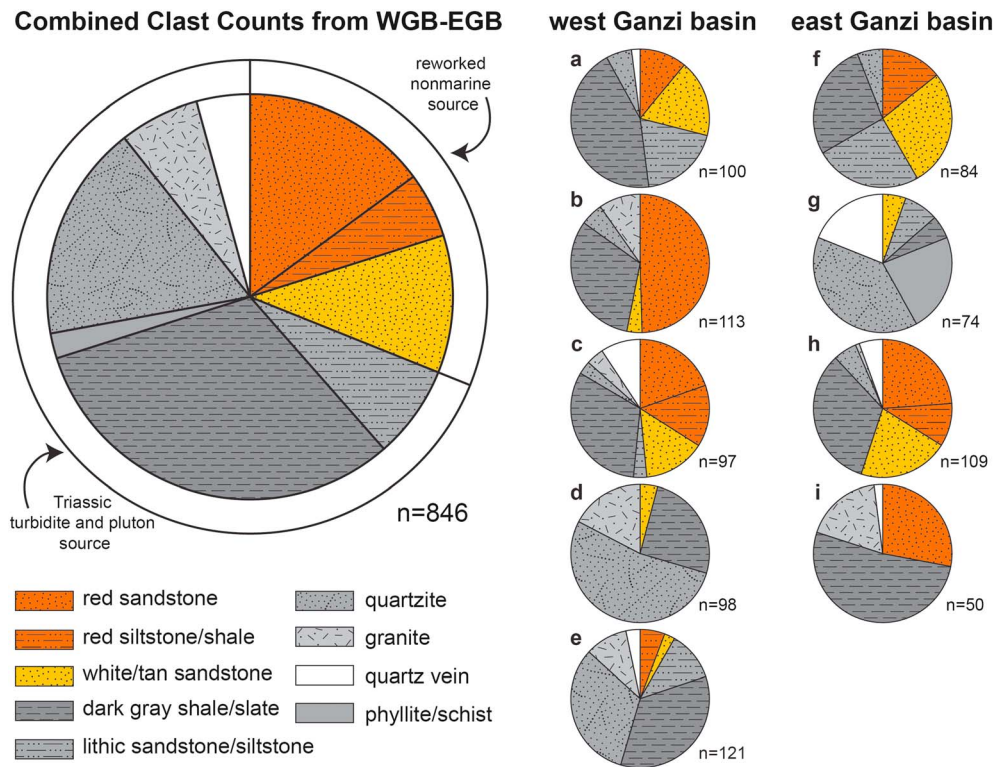
**Figure 4.** Field clast counts from conglomerate intrabeds in the west Ganzi basin and east Ganzi basin.

interbedded conglomerate and mudstone, with an overall fining upward trend. The WGB northeastern boundary reverse fault is oriented NNE-SSW, 49° ESE, and places Yidun Group turbidite rock over folded nonmarine strata (Figure 7b). The eastern and western WGB contacts could not be accessed; however, the color contrast between the red nonmarine strata and gray to dark-gray Triassic plutons and turbidite rocks allows for contact delineation using satellite imagery (Table S4). In the WGB, a right-lateral strike-slip fault trending ~300 offsets strata ~8 km in the central basin and cross-cuts older compressional features. Fault displacement dissipates toward the east, with no discernable expression in the EGB.
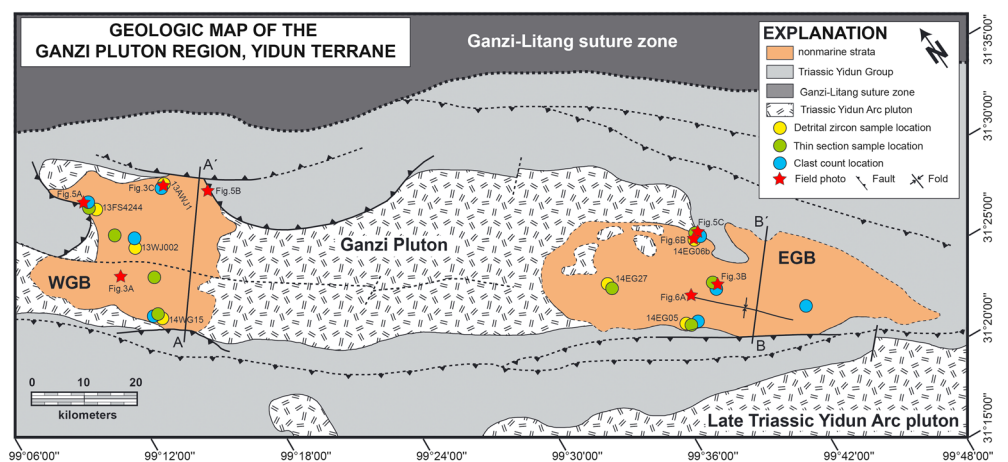


**Figure 5.** Simplified geologic map of the west Ganzi basin (WGB) and east Ganzi basin (EGB), northeastern Yidun terrane. Yellow circles and corresponding numbers correlate to detrital U-Pb zircon samples. Blue circles and numbers correlate to conglomerate clast counts. Green circles and corresponding numbers correlate to a thin section sample. Red stars indicate locations of field photographs corresponding to the noted figure. North is rotated at ~25°W.
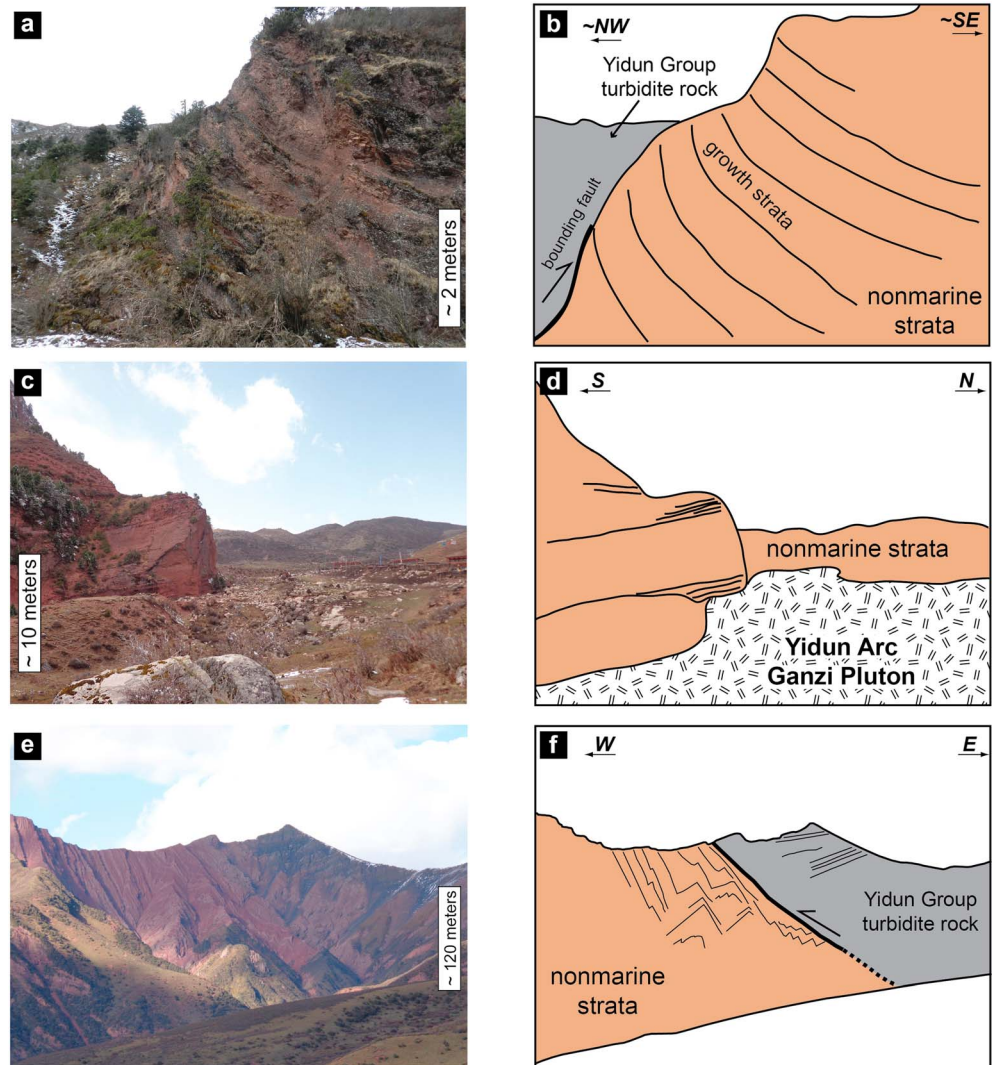
**Figure 6.** Examples of basin-boundary contacts in the west Ganzi basin (WGB) and east Ganzi basin (EGB). (a) Growth strata in the footwall of the WGB northern boundary thrust fault. (b) Corresponding illustration to Figure 7a. (c) Nonconformable contact between nonmarine strata and underlying Triassic Ganzi Pluton rock along the EGB northern basin boundary. (d) Corresponding illustration to Figure 7c. (e) The WGB thrust fault along the northeastern basin boundary, placing Triassic Yidun Group turbidite over tightly folded WGB nonmarine strata. (f) Corresponding illustration to Figure 7e. Locations of pictures are in Figure 6.

In the western EGB, the northern boundary is a nonconformity between EGB strata and the underlying granite of the Triassic Ganzi Pluton (Figure 7c), while the eastern part is characterized by an angular unconformity between EGB strata and the underlying, subvertically dipping Triassic Yidun Group turbidite rocks. The southern EGB boundary is a NW-SE trending reverse fault that places Triassic Yidun Group turbidite rocks over nonmarine strata. From northwest to southeast, the southwest-dipping fault plane changes dip from 57° to 85°. In places, the western EGB boundary is a nonconformity between nonmarine strata and the Ganzi Pluton, while elsewhere the boundary is an angular unconformity between the nonmarine strata and Yidun Group turbidite rocks. The eastern EGB boundary is an angular unconformity between the nonmarine strata and the Yidun Group turbidite rock.

Bedding orientations in both the WGB and EGB are variable because of internal folding; however, an average orientation is ~070, 33°SSE (Figure 8a). In the EGB, a ~5-km-long, ~0.5-km-wide syncline (Figure 8d), along with other smaller outcrop scale folds, plunges ~10–20° toward ~140–155. Nonaxial planar cleavage was measured within folded strata in the WGB. Analysis of fracture orientations combined with chronological
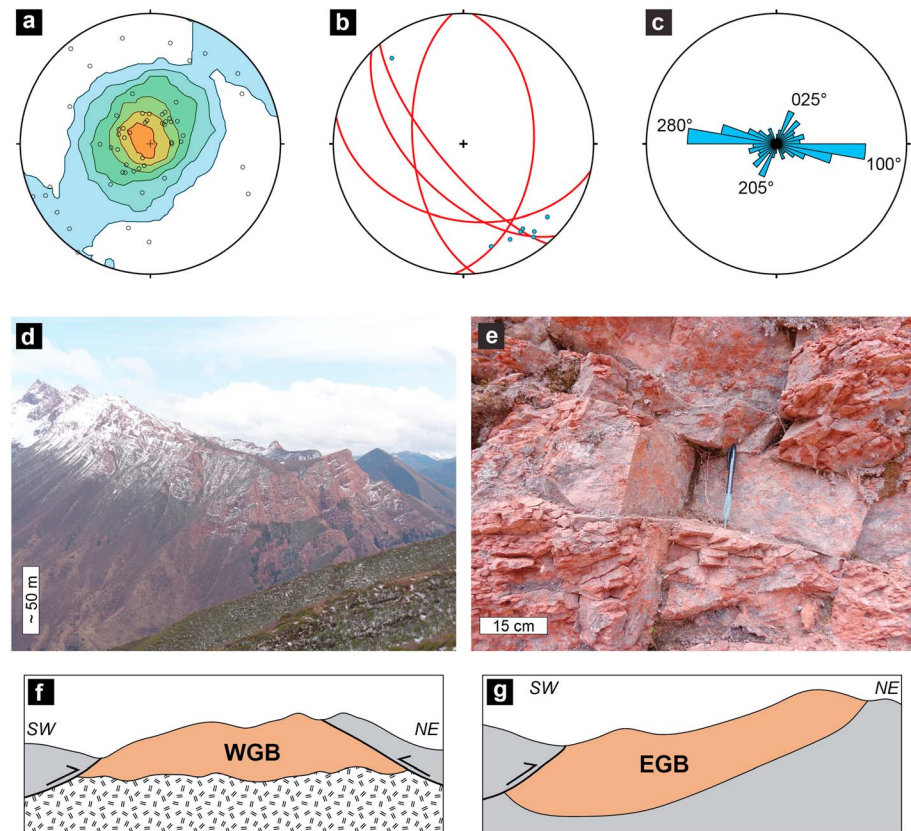
**Figure 7.** (a) Northern Hemisphere stereographic projection of bedding measurements. Measurements plotted as poles to bedding and contoured at the 2% level. (b) Stereographic representation of folds (poles) and faults (great circles) measured in the west Ganzi basin (WGB) and east Ganzi basin (EGB). (c) Rose diagram of fracture measurements in the WGB and EGB. (d) Basin scale syncline in the EGB (location shown in Figure 6). (e) Orthogonal fracture development in-between layers with low-angle fractures illustrating multiple generations of deformation. (f) Schematic cross section of the WGB. (g) Schematic cross section of the EGB. Location of both cross-section lines in Figure 6. Topographic profiles established through GeoMapApp 3.6.2 (http://www.geomapapp.org/).

relationships (i.e., abutting interfaces) reveals multiple fracture sets in the WGB and EGB (Figure 8e). A dominant ~E-W fracture set exists in the WGB and EGB that is the youngest fracture set, based on abutting relationships.

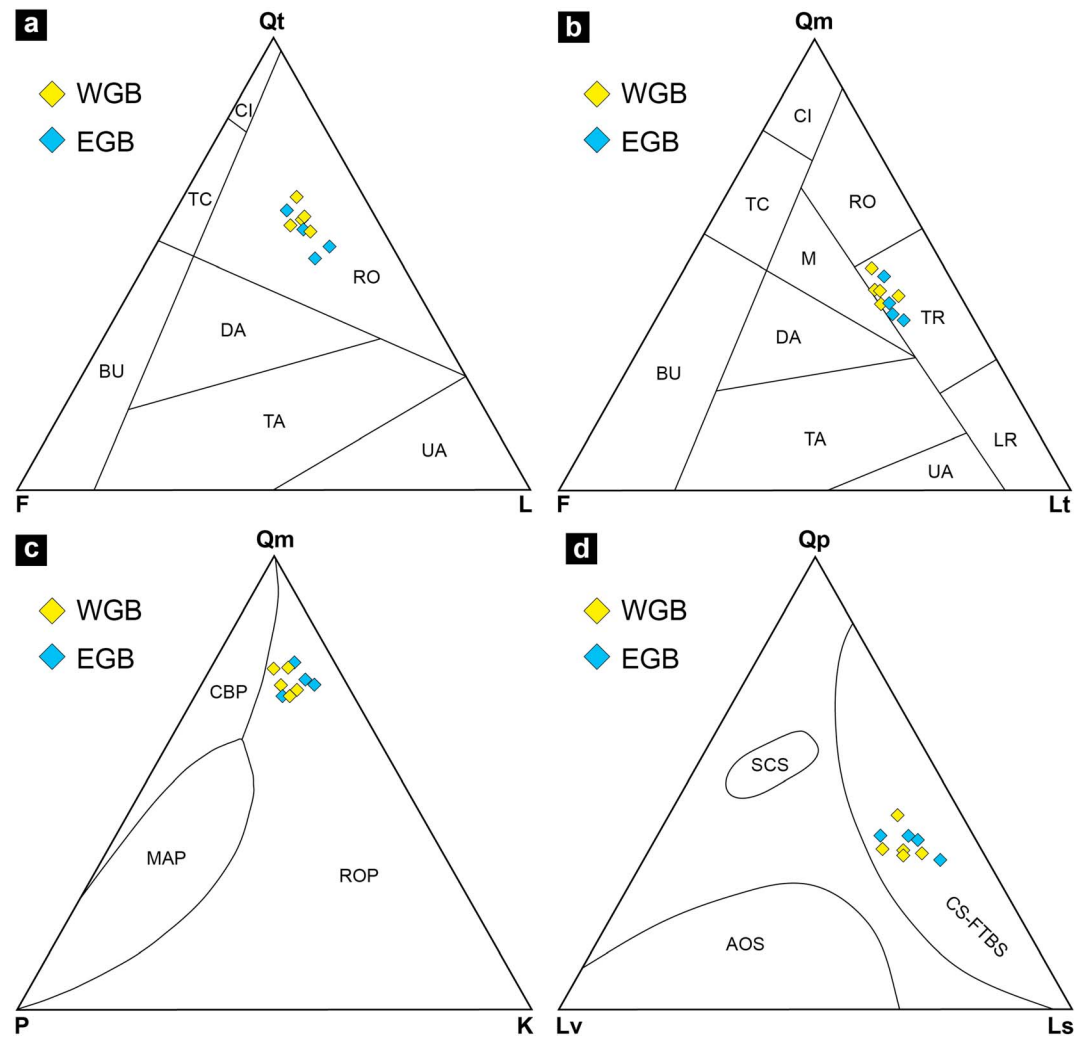### 4.3. Detrital U-Pb Zircon Geochronology

Detrital U-Pb zircon ages (n = 775) were collected from seven samples in the WGB and EGB (stratigraphic positions in Figure 3; geographic locations in Figure 6). Results illustrate major age peaks at 200–250, 250–300, 400–480, 720–880, 900–1,000, ~1,800, and ~2,400–2,500 Ma (Figure 9) with minor age peaks at 1,100–1,200 and 1,400–1,500 Ma.

#### 4.3.1. West Ganzi Basin

Sample 14WG15 is stratigraphically the highest sample in the WGB within unit 3 (Figure 9a). One hundred sixty-nine ages have concentrated age populations at 200–220, 450, ~950, ~1,800, and ~2,400 Ma. The youngest detrital U-Pb zircon population (n = 25) has a weighted mean average of 216.84 ± 0.86 Ma.

Sample 13AWJ1 is stratigraphically below 14WG15 and above 13FS4244 in the WGB, within the upper part of unit 2 (Figure 9b). Eighty-eight ages have concentrated age populations at ~2,500, ~1800, ~800–850, 450, and ~250 Ma. The youngest detrital U-Pb zircon population (n = 6) has a weighted mean average of 246 ± 11 Ma.

Sample 13FS4244 is stratigraphically below 13AWJ1 and above 13WJ002 in the WGB, within the lower part of unit 2 (Figure 9c). Eighty-nine ages have concentrated age populations at ~2,500, ~1800, ~800–850, and

**Figure 8.** Detrital U-Pb zircon geochronology results. Histogram bars represent 50-Ma intervals. Kernel density estimation curves calculated with a 15 bandwidth, normalized to area. Gray shaded areas represent corresponding age populations for multiple samples.

200–220 Ma. The youngest detrital U-Pb zircon population ($n = 20$) has a weighted mean average of 213.5 ± 2.4 Ma.

Sample 13WJ002 is stratigraphically the lowest sample collected in the WGB within unit 1 (Figure 9d). Ninety-two ages have concentrated age populations at ~2,400, ~1,800, ~1,600, ~1,200, ~950, ~550, 400–450, and 200–230 Ma. The youngest detrital U-Pb zircon population ($n = 6$) has a weighted mean average of 213.6 ± 6.9 Ma.

### 4.3.2. East Ganzi Basin
Sample 14EG06b is stratigraphically the highest sample collected in the EGB within unit 3 (Figure 9e). Eighty-eight ages have concentrated age populations at ~2,500, ~1,800, ~1,400, ~1,200, ~850, ~450, and 200–220 Ma. The youngest detrital U-Pb zircon population ($n = 7$) has a weighted mean average of 215.9 ± 1.5 Ma.

Sample 14EG27 is stratigraphically below 14EG06b and above 14EG05 in the EGB, within the upper part of unit 2 (Figure 9f). Eighty-six ages have concentrated age populations at ~2,500, ~1,800, ~800–850, 450, and ~250 Ma. The youngest detrital U-Pb zircon population ($n = 6$) has a weighted mean average of 238.9 ± 9.0 Ma.
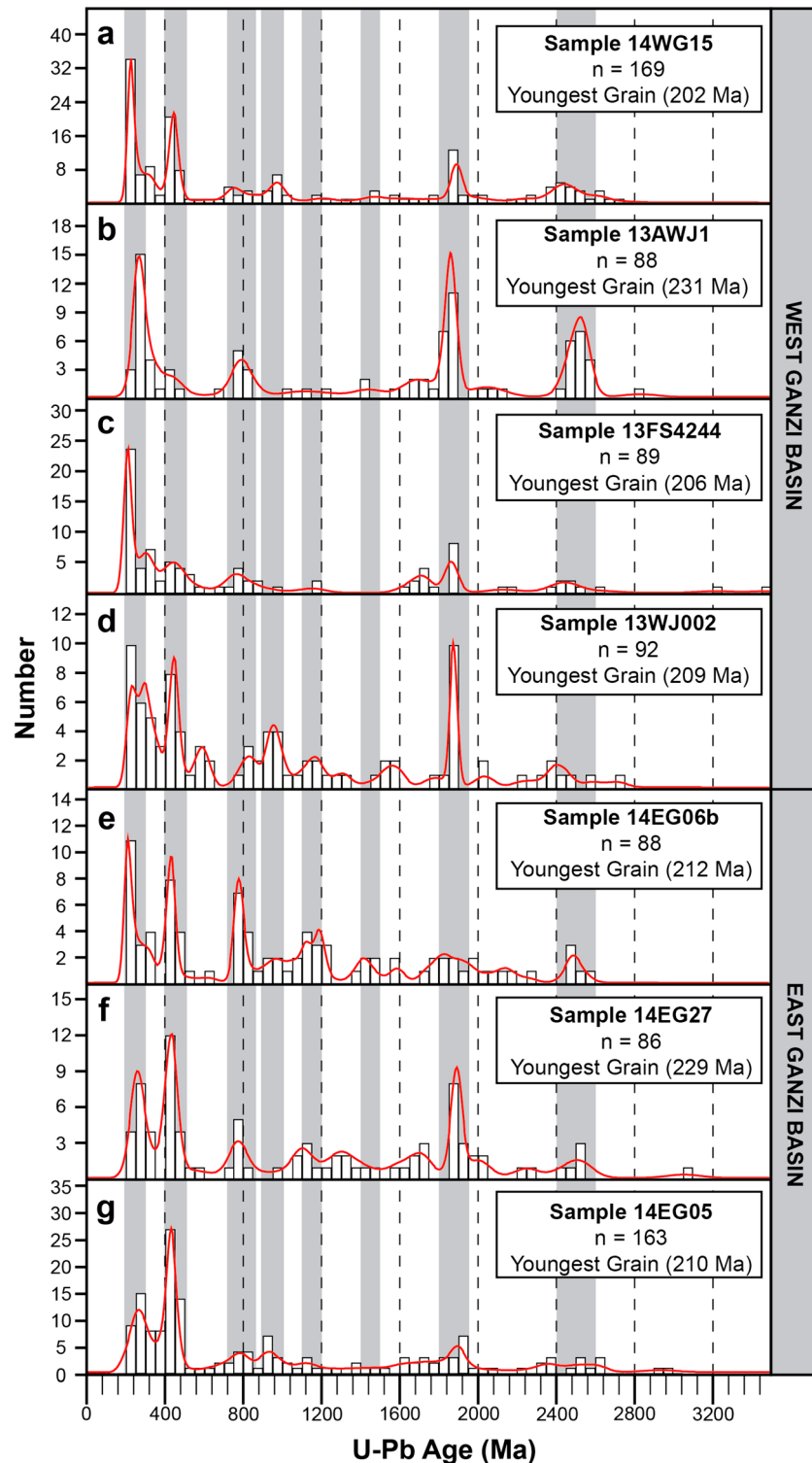
**Figure 9.** Petrographic results from nine samples. (a) Total quartz-feldspar-lithics plot: CI = craton interior, TC = transitional continental, BU = basement uplift, RO = recycled orogenic, DA = dissected arc, TA = transitional arc, UA = undissected arc. (b) Monocrystalline quartz-feldspar-total lithics plot: CI = craton interior, TC = transitional continental, BU = basement uplift, RO = recycled orogenic, M = mixed, DA = dissected arc, TA = transitional arc, TR = transitional recycled, LR = lithic recycled, UA = undissected arc. (c) Monocrystalline quartz-plagioclase-potassium feldspar plot: CBP = continental block provenance, MAP = magmatic arc provenance, ROP = recycled orogen provenance. (d) Polycrystalline quartz-volcanic lithics-sedimentary lithics plot: SCS = subduction complex sources, AOS = arc orogen source, CS-FTBS = collision suture and fold-thrust belt sources.
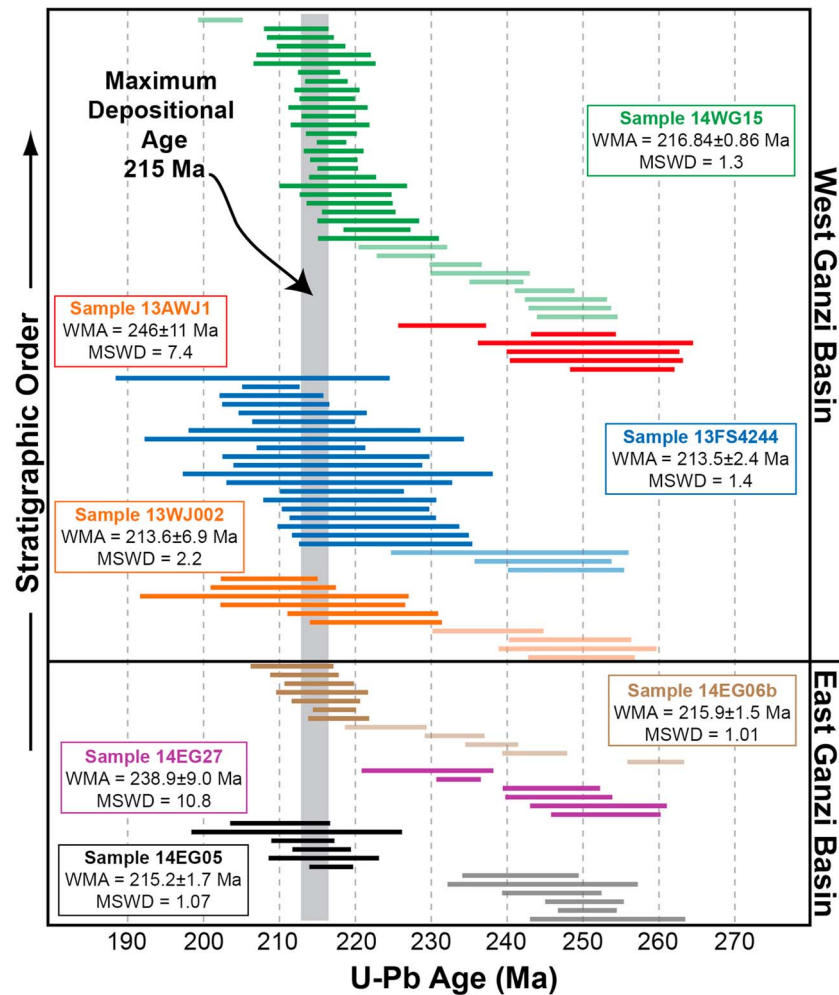
**Figure 10.** Detrital U-Pb zircon geochronology results illustrating a maximum depositional age of ~215 Ma for the west Ganzi basin (WGB) and east Ganzi basin (EGB). The maximum depositional age was determined by calculating a weighted mean average (WMA) of the youngest zircon population from each sample. Samples are ordered based on the specific basin and stratigraphic position. Every detrital U-Pb zircon that yielded an age between 200 and 260 Ma is plotted, with the bold colored bars indicating the grains that were included in the weighted mean average calculation. Statistics for each sample are indicated in the corresponding colored box. Bars represent $2\sigma$ error. MSWD = mean square weighted deviation.

Sample 14EG05 is stratigraphically the lowest sample collected in the EGB, within the lower part of unit 2 (Figure 9g). One hundred sixty-three ages have concentrated age populations at ~2,500, ~1800, ~800–850, 450, and ~250 Ma. The youngest detrital U-Pb zircon population ($n = 6$) has a weighted mean average of 215.2 ± 1.7 Ma.

## 4.4. Thin Section Petrology

Minerals present include monocrystalline quartz, polycrystalline quartz, plagioclase feldspar, potassium feldspar, volcanic/meta-volcanic lithic fragments, and sedimentary/meta-sedimentary lithic fragments. Framework-grain modal compositions of all nine samples are plotted in the recycled orogenic field of the total quartz-feldspar-lithics provenance discrimination ternary diagram (Figure 10a), the transitional recycled field for the monocrystalline quartz-feldspar-total lithics provenance discrimination ternary diagram (Figure 10b), the recycled orogen provenance for the monocrystalline quartz-plagioclase-potassium feldspar provenance discrimination ternary diagram (Figure 10c), and the collision suture and fold-thrust belt sources field for the polycrystalline quartz-volcanic lithics-sedimentary lithics provenance discrimination ternary diagram (Figure 10d).
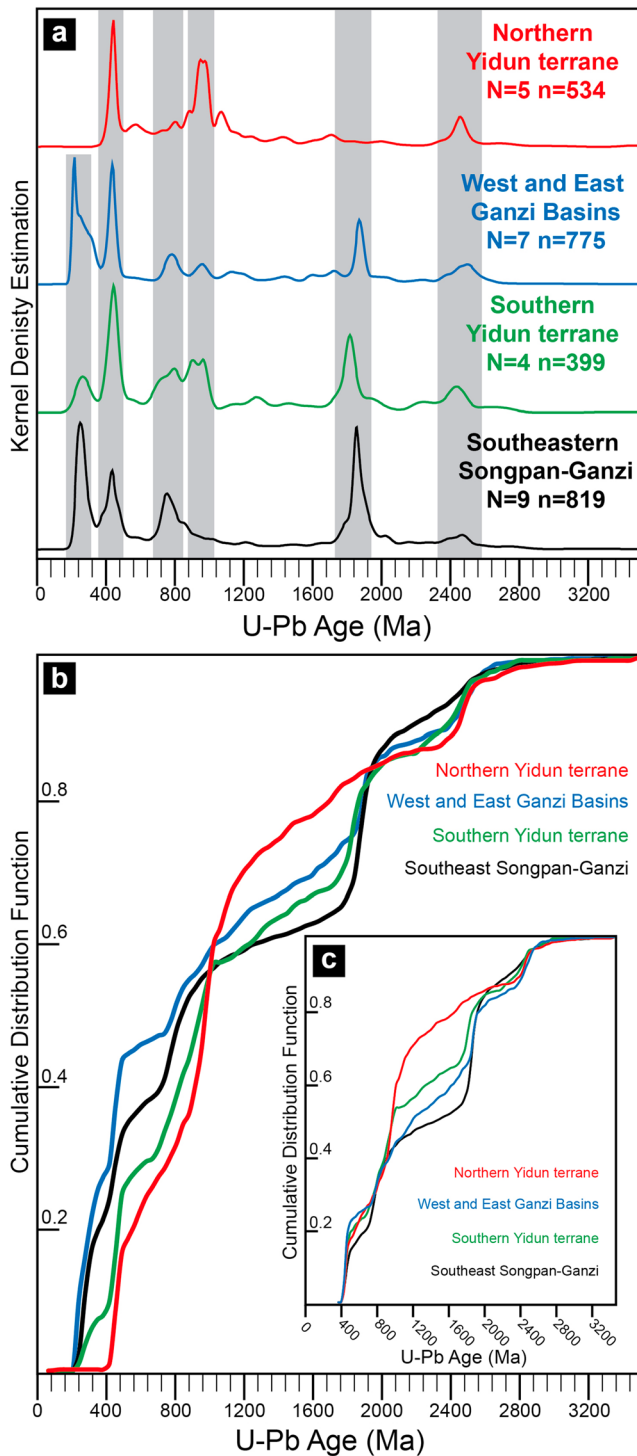
**Figure 11.** (a) Kernel density estimation curves (15 bin size) for a composite of all seven samples from Figure 9: west Ganzi basin-east Ganzi basin (WGB-EGB), northern Yidun terrane turbidites, southern Yidun terrane turbidites, and SE Songpan-Ganzi turbidites. Gray shaded areas represent corresponding age populations. (b) Cumulative density plots (CDP) for the WGB-EGB, northern Yidun terrane turbidites, southern Yidun terrane turbidites, and SE Songpan-Ganzi turbidites. (c) CDP curves from same data in (a) and (b), excluding all grains <400 Ma.

# 5. Interpretations

## 5.1. Age of WGB and EGB Strata

When positioned in stratigraphic succession, the weighted mean averages from the youngest detrital U-Pb zircon population in the WGB and EGB illustrate a coherent MDA of ~215 Ma (Figure 11). In addition, Figure 11 illustrates that each basin contains one sample, located in the middle to the upper portion of basin stratigraphy (unit 2), which produces a MDA of ~238–246 Ma. The correlation of MDAs supports an interpretation that both basins were deposited coevally within the same system. However, a MDA of ~215 Ma is slightly older than the stratigraphically youngest formation in the Yidun Group, the Lamaya Formation (203–199 Ma; Bureau of Geology and Mineral Resources of Sichuan Province, 1991; Wang, Zhou, et al., 2013). Because the Yidun Group is a primary sediment source for the WGB and EGB strata, it suggests that the true depositional age for the WGB and EGB is younger than the calculated MDA indicated by detrital U-Pb zircon geochronology. Cretaceous palynology results (Liu, 1999) also suggests a younger depositional age for the WGB and EGB nonmarine strata.

Thermochronology results from the Triassic Daocheng Pluton, located in the southern Yidun terrane, illustrate two cooling phases at Late Jurassic-Early Cretaceous and late Oligocene-early Miocene time (Clark et al., 2005; Tian et al., 2014). Jackson et al. (2018) suggest that a Cenozoic MDA of ~45 Ma for the Mula basin, which directly overlies the Daocheng Pluton, integrates well with a late Oligocene-early Miocene timing for basin development. We interpret the ~215-Ma MDA for the WGB and EGB to correlate to the Late Jurassic-Early Cretaceous cooling phase from the Daocheng Pluton. While not definitive evidence for assigning a stratigraphic age, the lack of 190–165 Ma zircon from Bangong Arc volcanism (Guynn et al., 2006) and 105–90 Ma zircon from the Cheur Pluton (Reid et al., 2007), located ~25 km west of the WGB, seems to collaborate nonmarine deposition during Late Jurassic through Middle Cretaceous time. Therefore, based on a ~215-Ma MDA for the WGB and EGB, regional U-Pb zircon geochronology, thermochronology from the Yidun terrane, and previously reported Cretaceous palynology results, we interpret a Late Jurassic through Middle Cretaceous depositional age for nonmarine strata in the WGB and EGB.

## 5.2. Sediment Provenance

Thin section petrology and field clast counts indicate that the strata are from a recycled orogenic source. Conglomerate clast counts also indicate that the strata are from Triassic Yidun Group, Triassic Yidun Arc, and recycled nonmarine strata. To further discriminate the provenance of the strata, we compare detrital U-Pb zircon results and previously published regional curves.

The detrital U-Pb zircon signature of the Triassic Yidun Group strata immediately adjacent to the Ganzi basin, referred to as the northern Yidun Group by Wang, Wang, Chen, et al. (2013) and Ding et al. (2013), lacks the Early Triassic grains. However, northern Yidun Group rocks do contain Paleozoic (~450 Ma) grain ages along with abundant late Mesoproterozoic (~1.0 Ga) grain ages and a small population of Archean (~2.5 Ga) grain ages. These age populations appear in the WGB and EGB and could have originated from a northern Yidun Group source. Rocks of the southern Yidun Group do show a small population of Early Triassic ages
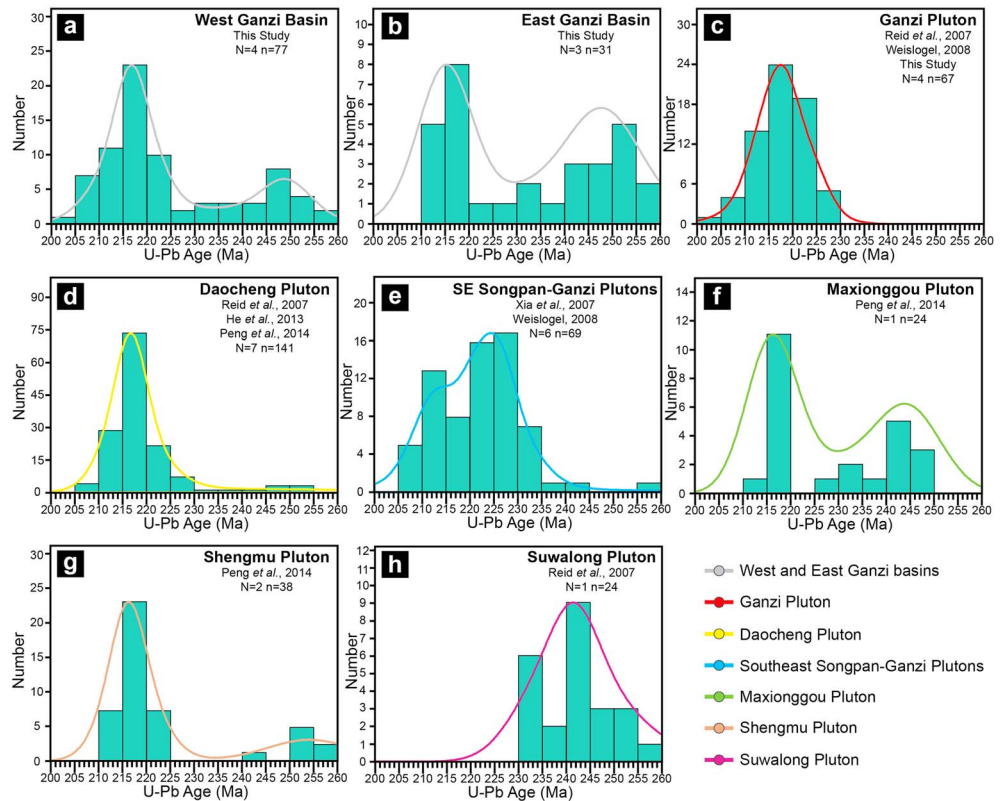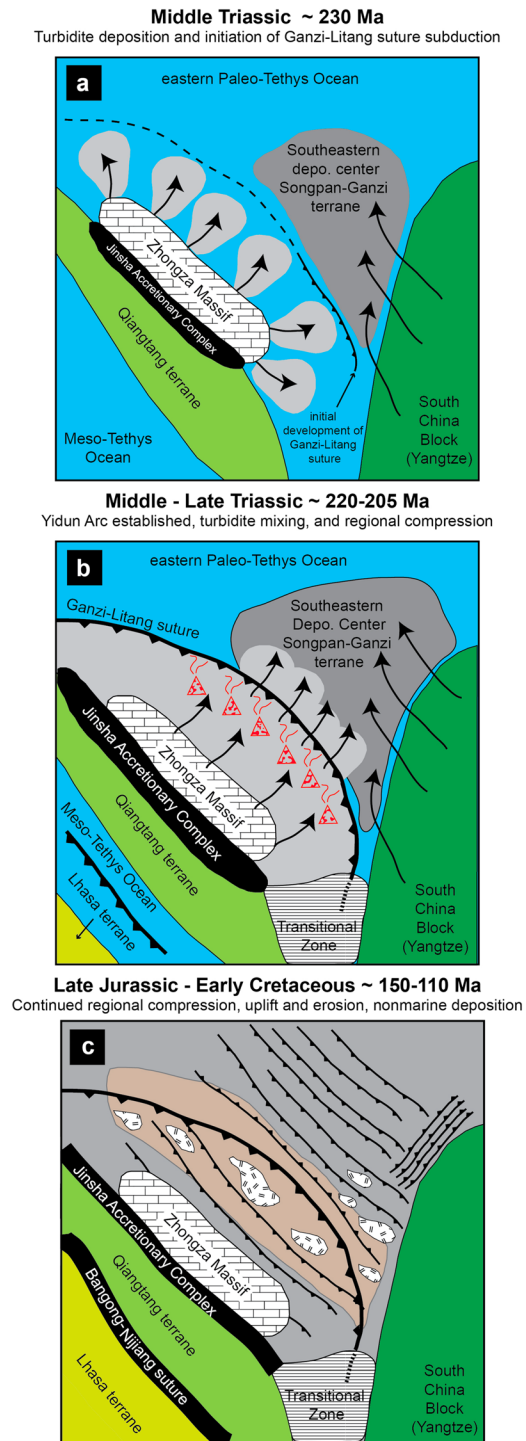
**Figure 12.** Calculated U-Pb ages for plutons in the Yidun and southeastern Songpan-Ganzi terranes (geographic locations shown in Figure 2 and in supporting information). Histogram bars and kernel density estimation curve for (a) 200–260-Ma WGB grains, (b) 200–260-Ma EGB grains, (c) Ganzi Pluton, (d) Daocheng Pluton, (e) plutons located in the southeastern Songpan-Ganzi terrane, (f) Maxionggou Pluton, (g) Shengmu Pluton, and (h) Suwalong Pluton.

(240–250 Ma) as well as Neoproterozoic ages (~800 Ma), which are present in the WGB and EGB but absent in northern Yidun Group. In addition, the southern Yidun Group contains Paleozoic (~450 Ma), Neoproterozoic (~750 Ma), and Paleoproterozoic (~1.8 Ga) ages and a small cluster of Archean (~2.5 Ga) grains, ages that are all present in the WGB and EGB. However, a southern Yidun Group source would require a large sedimentary transport system that would also have likely included zircon from Cretaceous magmatic rocks. One possibility is that the southern Yidun Group strata were adjacent to the Ganzi basins during late Mesozoic-early Cenozoic deposition and served as sources of sediment and later were translated southeastward by Cenozoic strike-slip fault deformation.

Comparison of regional detrital U-Pb zircon geochronology curves illustrates the difference and similarities between the Triassic Yidun Group from the southern and northern parts of the Yidun terrane, Triassic turbidite rocks from the Songpan-Ganzi terrane's southeastern depocenter, and WGB and EGB nonmarine strata (Figure 12). The WGB and EGB curves are most dissimilar to the northern Yidun Group turbidite curve, rocks that the WGB and EGB overlie and are in fault contact with. Because of the lack of <400-Ma grains in the northern Yidun Group curve, Figure 12c compares the four curves with only grains >400 Ma, where a difference between WGB and EGB nonmarine strata to the northern Yidun turbidites remains the most dissimilar. Kolmogorov-Smirnov statistical tests on the regional curves indicate that the WGB and EGB curves are most similar to the southern Yidun terrane and Songpan-Ganzi southeastern depocenter turbidite curves. These data suggest that WGB and EGB sediments were sourced from a mixture of Triassic Yidun Group, Yidun Arc, and Songpan-Ganzi rocks.

Triassic zircons (108 grains), presumably derived from Yidun Arc plutons, make up the youngest detrital U-Pb zircon age population(s) at ~216 and ~249 Ma in the WGB and EGB, respectively (Figures 13a and 13b). The Late Triassic age peak matches within error to the age peak of zircon ages obtained for the underlying Yidun Arc Ganzi Pluton, which has been dated at ~218 Ma (Reid et al., 2007; Weislogel, 2008; Figure 13c). Other

**Middle Triassic ~ 230 Ma**
Turbidite deposition and initiation of Ganzi-Litang suture subduction

**Middle - Late Triassic ~ 220-205 Ma**
Yidun Arc established, turbidite mixing, and regional compression

**Late Jurassic - Early Cretaceous ~ 150-110 Ma**
Continued regional compression, uplift and erosion, nonmarine deposition

**Figure 13.** Tectonic model for the development of the Mesozoic WGB and EGB in the northern Yidun terrane. (a) Erosion of the Zhongza Massif and South China Block and transport and deposition of turbidite rocks in the eastern branch of the Paleo-Tethys Ocean, which coincided with the initiation of subduction along the Ganzi-Litang suture. (b) Formation of the Triassic Yidun Arc and mixing of Yidun and Songpan-Ganzi terrane turbidite rocks in the eastern Paleo-Tethys Ocean. (c) Regional contractional deformation resulting from the Lhasa-Qiangtang collision; aerial exposure of Triassic turbidite and plutonic rocks; and erosion, regional transport, and deposition of nonmarine strata associated coevally with further contractional deformation.

Yidun Arc plutons, including the largest, the Daocheng Pluton located to the south-southeast of the WGB and EGB, are also dated at 215–220 Ma (He et al., 2013; Figure 13d). However, grains older than 230 Ma in the WGB and EGB cannot be sourced from the local Ganzi Pluton. Identifying the origin of these grains is difficult because zircon of this age are present both in surrounding plutons as well as in the flanking Yidun Group and Songpan-Ganzi complex strata (southeastern depocenter). Plutons of the Jiangda-Weixi Arc to the south-southwest that intrude the Jinsha Accretionary Complex and Zhongza Massif in the western portion of the Yidun terrane contain ages from 230 to 270 Ma with an age peak at ~242 Ma (Peng et al., 2014; Reid et al., 2007; Figure 13h). The plutons of the Yidun Arc range in age from 210 to 260 Ma (e.g., Peng et al., 2014). It is possible that the materials were eroded from these igneous rocks and transported into the WGB and EGB; however, it is likely that any sizeable sedimentary transport system capable of routing sediment from plutons to the north or south would have also included Cretaceous zircons. Alternatively, multiple plutons in the southeastern Songpan-Ganzi depocenter have ages ranging from 205 to 235 Ma and contain two age peaks at ~212 and ~225 Ma (Weislogel, 2008; Xiao et al., 2007; Figure 13e). The southeastern Songpan-Ganzi turbidites also contain detrital U-Pb zircon signatures that show Triassic age peaks at 240–250 Ma (Weislogel et al., 2010). It is possible that exhumed rocks from southeastern Songpan-Ganzi terrane were eroded and contributed to the Triassic ages, as well as the late Paleozoic, Neoproterozoic, Paleoproterozoic, and Archean grains in the WGB and EGB.

We interpret the WGB and EGB basin fill to have been sourced regionally, in a large drainage system from the southern Yidun terrane and the southeastern depocenter of the Songpan-Ganzi terrane. However, our interpretation of a regional drainage system may be overestimated in size, in that prior to Cenozoic southeastward extrusion of crustal material (e.g., Wang & Burchfiel, 2000), the southern Yidun terrane and Songpan-Ganzi terrane turbidite rocks may have been positioned more proximal to the WGB and EGB, therefore representing a more local sediment source. In either case, it remains clear that the northern Yidun Group turbidite and Late Triassic Ganzi Pluton rocks lack the zircon populations to account for the spectrum of ages in the WGB and EGB data.

### 5.3. Tectonic Setting

Documentation of late Mesozoic tectonism in the Yidun terrane has focused on underformed Cretaceous plutonic bodies that intrude the Triassic Yidun Group. Reid et al. (2007) suggest that Late Cretaceous (~105–95 Ma) plutonic bodies throughout the Yidun terrane are related to the northward subduction of the Neo-Tethys oceanic crust, which manifested as a result of upper-crustal regional extension. However, we interpret that the WGB and EGB formed in a contractional deformational regime based on reverse fault contacts along basin boundaries with associated footwall growth strata, as well as the parallel trend of fold-axes to basin bounding faults. Tian et al. (2014) document an episode of Late Jurassic-Early Cretaceous regional cooling in the Yidun and Songpan-Ganzi terranes from thermochronology and interpret the results to correspond to contractional tectonics related to the Lhasa-Qiangtang collision. Therefore, we suggest that the WGB and EGB

document the development of a Mesozoic foreland, located near the Ganzi-Litang suture. In this model (Figure 13), exhumation resulting from upper-crustal shortening began in the southern part of the Yidun terrane and Songpan-Ganzi terrane leading to erosion of Triassic turbidite and plutonic rock. A regional drainage system was subsequently established as shortening continued, which allowed for sediment to be transported and deposited on top of Triassic Ganzi Pluton and Yidun Group rocks in the northern part of the terrane. The strike-slip fault in the WGB is interpreted to have developed in Cenozoic time after basin formation, associated with a network of faults that promoted extrusion and clockwise rotation of eastern Tibetan Plateau crustal material (Burchfiel et al., 1995; Clark et al., 2005; Wang & Burchfiel, 1997, 2000).

## 6. Discussion

### 6.1. Mesozoic Versus Cenozoic Nonmarine Strata in the Yidun Terrane

With these data and the southern Yidun terrane Mula basin data (Jackson et al., 2018), a comparison between Mesozoic and Cenozoic nonmarine deposits throughout the eastern Tibetan Plateau can be explored. The primary difference is the stratigraphic age for the northern (Mesozoic) and southern (Cenozoic) Yidun terrane nonmarine basins. A Cenozoic age for the Mula basin is based on detrital U-Pb zircon geochronology and previously reported thermochronology results that show a cooling phase in late Oligocene-early Miocene time (Clark et al., 2005; Tian et al., 2014). Jackson et al. (2018) calculated a MDA of ~45 Ma for the Mula basin, while we calculated a MDA of ~215 Ma for the WGB and EGB from the weighted mean average of the youngest zircon population(s). The difference in MDA for the WGB and EGB compared to the Mula basin, in conjunction with previously reported Cretaceous palynology results from the WGB, correlates well with the Late Jurassic-Early Cretaceous cooling phase present in thermochronology results in the Yidun terrane (Clark et al., 2005; Tian et al., 2014).

The WGB and EGB as well as the Mula basin indicate a development associated with contractional deformation. However, growth strata in the footwall of basin-bounding faults are only found in the WGB and EGB. The absence of growth strata in the Cenozoic Mula basin substantiates the lag time between the geochronology and thermochronology results stated above, which indicate that movement along the basin-bounding fault post-dates deposition and that Mula basin fill was eroded from preexisting source rocks. In contrast, the growth strata in the Mesozoic WGB and EGB indicate that basin infilling was coeval with fault movement.

The overall stratigraphic architecture is similar between the Cenozoic Mula basin and the Mesozoic WGB and EGB, with a lower, dominantly conglomeratic unit (unit 1 for the WGB, EGB, and Mula basin), overlain by a finer-grained mudstone dominated succession with siltstone and sandstone interbeds (unit 2 for the WGB, EGB, and Mula basin). The difference in stratigraphic architecture is present in unit 3 for the WGB/EGB and Mula basin. In the Mula basin, unit 3 consists of fine-grained mudstone and shale, interbedded with small (<1-m-thick) siltstone to fine-grained sandstones, thus continuing the upward-fining trend of basin stratigraphy. In the WGB and EGB, unit 3 consists of interbedded sandstones and mudstones, a massive (~150-m-thick) fine-grained sandstone, capped by interbedded conglomerate and mudstone, representing a coarsening-upward trend at the top of basin stratigraphy.

The shape of the Mesozoic WGB and EGB differs from that of the Cenozoic Mula basin. The Mula basin is narrow and elongate in shape, parallel to the basin's bounding thrust fault along the eastern border. The WGB and EGB express more ellipsoidal geometric shapes that presumably result from erosion and are not representative of the basin formation geometry. While subsequent deformational overprinting may have obscured the original shape of the WGB and EGB, it seems that only localized strike-slip faulting along the Ganzi fault has offset the WGB ~5–10 km, representing only minor reconfiguration of the overall basin shape.

A difference in sedimentary provenance is also indicated between the Mesozoic WGB and EGB and Cenozoic Mula basin. Provenance results from the Mula basin indicate a local sediment source, while the WGB and EGB illustrate a regional sediment source. The regional sediment source for the Mesozoic WGB and EGB presumably distinguishes the northern Yidun terrane nonmarine strata from conventional Cenozoic nonmarine exposures throughout the eastern Tibetan Plateau and may be interpreted to indicate more expansive exhumation and deformation during Mesozoic time compared to the localized uplifts and sediment source signatures associated with the Cenozoic Mula basin.

### 6.2. Broader Implications

Many studies note that the current crustal thickness of the eastern Tibetan Plateau (~60 km) inherited some thickness from Mesozoic tectonism (Robert et al., 2010; Wang et al., 2007; Xu et al., 2007). Understanding this pre-Cenozoic thickening of the crust is essential to determining the processes involved in forming the present day crustal thickness. Throughout the Tibetan Plateau, evidence for Cretaceous deformation and rapid cooling histories associated with compression resulting from the Lhasa and Qiangtang collision are well documented (DeCelles et al., 2007; Hetzel et al., 2011; Kapp et al., 2005, 2007; Murphy et al., 1997; Rohrmann et al., 2012; Zhang et al., 2012; Wang et al., 2014). Recently, Shang (2016) documented Cretaceous strata, which resemble WGB and EGB strata, in the Qamdo basin of the Qiangtang terrane and interpreted a Jomda-Weixi arc (Jinsha Accretionary Complex) sediment source. These studies all suggest that foreland basins developed in front (to the north) of the Lhasa-Qiangtang collision, which produced upper-crustal shortening and thickening throughout the plateau. The recognition of the WGB and EGB as foreland basin deposits in response to the Lhasa-Qiangtang collision advances our understanding of the temporal and spatial developments of the pre-Cenozoic deformation and deposition throughout the eastern Tibetan Plateau.

## 7. Conclusions

Our investigation of the WGB and EGB in the northern Yidun terrane yields the following conclusions:

1. The WGB consists of ~800 m and the EGB consists of ~1,300–1,600 m of nonmarine strata deposited in alluvial environments. Basin stratigraphic architecture can be separated into three units based primarily on grain size.
2. Basin boundaries in the WGB and EGB are characterized by reverse fault and unconformable contacts between Triassic Ganzi Pluton (Yidun Arc) and Triassic Yidun Group turbidite rock to nonmarine strata. Reverse faults, growth strata along basin boundaries, and internal basin deformation show that nonmarine deposition occurred syntectonically in a contractional tectonic setting.
3. A MDA of ~215 Ma, calculated from youngest detrital zircon populations, brackets a Mesozoic or younger age for the WGB and EGB. Detrital U-Pb zircon geochronology from this study along with previously reported Cretaceous palynology ages and Cretaceous thermochronology cooling ages from the Yidun Arc demonstrates a Cretaceous age for nonmarine strata.
4. Detrital zircon geochronology, conglomerate clast counts, and thin section petrology data indicate that the WGB and the EGB strata were sourced regionally from southern Yidun terrane and southeastern Songpan-Ganzi turbidite rock, along with influx from Yidun Arc plutonic rock. A large, northwestwardly directed drainage network established at the time of basin development is interpreted. Because of the similarity of ages in multiple Yidun Arc plutons throughout the Yidun and southeastern Songpan-Ganzi terranes, spatial identification of specific plutonic sources remains elusive.
5. The WGB and the EGB developed in a foreland basin associated to the collision between the Lhasa and Qiangtang terranes, which manifested in upper-crustal shortening, exhumation, and erosion of predeformed Triassic turbidite rock and undeformed Triassic plutonic bodies throughout the Yidun and southern Songpan-Ganzi terranes.

## References

Burchfiel, B. C., & Chen, Z. (2012). Tectonics of the southeastern Tibetan Plateau and its adjacent foreland. *Geological Society of America Memoir*, *210*, 231.

Burchfiel, B. C., Chen, Z., Liu, Y., & Royden, L. H. (1995). Tectonics of the Longmen Shan and adjacent regions. *International Geology Review*, *37*(8), 661–735. https://doi.org/10.1080/00206819509465424

Bureau of Geology and Mineral Resources of Sichuan Province (1991). *Regional geology of Sichuan province, Geological Memoirs of PRC Ministry of Geology and Mineral Resources*, (p. 730). Beijing: Geological Publishing House. (In Chinese with English Summary).

Clark, M. K., Bush, J. W. M., & Royden, L. H. (2005). Dynamic topography produced by lower crustal flow against rheological strength heterogeneities bordering the Tibetan Plateau. *Geophysical Journal International*, *162*(2), 575–590. https://doi.org/10.1111/j.1365-246X.2005.02580.x

Chen, Z., & Chen, X. (1987). On the tectonic evolution of the west margin of the Yangzi Block: Chengdu Intitute of Geology and Mineral Resources (171 p.).

Craddock, W. H., Kirby, E., Dewen, Z., & Jianhui, C. (2012). Tectonic setting of Cretaceous basins on the NE Tibetan Plateau: Insights from the Jungong basin. *Basin Research*, *24*(1), 51–69. https://doi.org/10.1111/j.1365-2117.2011.00515.x

DeCelles, P. G., Kapp, P., Ding, L., & Gehrels, G. E. (2007). Late Cretaceous to middle Tertiary basin evolution in the central Tibetan Plateau: Changing environments in response to tectonic partitioning, aridification, and regional elevation gain. *Geological Society of America Bulletin*, *119*(5-6), 654–680. https://doi.org/10.1130/B26074.1

DeCelles, P. G., Kapp, P., Gehrels, G. E., & Ding, L. (2014). Paleocene-Eocene foreland basin evolution in the Himalaya of southern Tibet and Nepal: Implications for the age of initial India-Asia collision. *Tectonics*, *33*, 824–849. https://doi.org/10.1002/2014TC003522

Dehler, C. M., Fanning, C. M., Link, P. K., Kingsbury, E. M., & Rybczynski, D. (2010). Maximum depositonal age and provenance of the Uinta Mountain Group and Big Cottonwood Formation, northern Utah: Paleogeography of rifting western Laurentia. *Geological Society of America Bulletin*, *122*, 1686–1699.

Dewey, J., Shackleton, R., Chang, C. F., & Sun, Y. Y. (1988). The tectonic evolution of the Tibetan Plateau. *Philosophical Transactions of the Royal Society of London*, *327*(1594), 379–413. https://doi.org/10.1098/rsta.1988.0135

Dickinson, W. R. (1970). Interpreting detrital modes of greywacke and arkose. *Journal of Sedimentary Petrology*, *40*, 695–707.

Dickinson, W. R. (1985). Interpreting provenance relations from detrital modes of sandstones. In G. G. Zuffa (Ed.), *Provenance of arenites*, (pp. 333–361). Boston: D. Reidel Publishing.

Dickinson, W. R., & Gehrels, G. E. (2003). U-Pb ages of detrital zircons from Permian and Jurassic eolian sandstones of the Colorado Plateau, USA; Paleogeographic implications. *Sedimentary Geology*, *163*, 29–66.

Dickinson, W. R., & Gehrels, G. E. (2009a). Use of U-Pb ages of detrital zircons to infer maximum depositional ages of strata: A test against a Colorado Plateau Mesozoic database. *Earth and Planetary Science Letters*, *288*(1-2), 115–125. https://doi.org/10.1016/j.epsl.2009.09.013

Dickinson, W. R., & Gehrels, G. E. (2009b). U-Pb ages of detrital zircons in Jurassic eolian and associated sandstones of the Colorado plateau: Evidence for transcontinental dispersal and intraregional recycling of sediment. *Geological Society of America Bulletin*, *121*(3-4), 408–433. https://doi.org/10.1130/B26406.1

Dickinson, W. R., & Suczek, C. (1979). Plate tectonics and sandstone compositions. *American Association of Petroleum Geologists Bulletin*, *63*, 2164–2182.

Ding, L., Yang, D., Cai, F. L., Pullen, A., Kapp, P., Gehrels, G. E., et al. (2013). Provenance analysis of the Mesozoic Hoh-Xil-Songpan-Ganzi Turbidites in northern Tibet: Implications for the tectonic evolution of the eastern Paleo-Tethys Ocean. *Tectonics*, *32*, 34–48. https://doi.org/10.1002/tect.20013

Enkelmann, E., Weislogel, A., Ratschbacher, L., Eide, E., Renno, A., & Wooden, J. (2007). How was the Triassic Songpan-Ganzi basin filled? A provenance study. *Tectonics*, *26*, TC4007. https://doi.org/10.1029/2006TC002078

Gehrels, G., Valencia, V., & Pullen, A. (2006). Detrital zircon geochronology by laser-ablation multicollector ICPMS at the Arizona LaserChron Center. In T. Loszewski & W. Huff (Eds.), *Geochronology: Emerging opportunities*, *Paleontological Society Papers*, (Vol. 12, pp. 67–76). Philadelphia, PA: The Paleontological Society.

Gehrels, G. E., Valencia, V., & Ruiz, J. (2008). Enhanced precision, accuracy, efficiency, and spatial resolution of U-Pb ages by laser ablation-multicollector-inductively coupled plasma-mass spectrometry. *Geochemistry, Geophysics, Geosystems*, *9*, Q03017. https://doi.org/10.1029/2007GC001805

Guynn, J. H., Kapp, P., Pullen, A., Heizler, M., Gehrels, G., & Ding, L. (2006). Tibetan basement rocks near Amdo reveal "missing" Mesozoic tectonism along the Bangong suture, central Tibet. *Geology*, *34*(6), 505–508.

Harrowfield, M. J., & Wilson, C. J. L. (2005). Indosinian deformation of the Songpan Garze fold belt, northeast Tibet Plateau. *Journal of Structural Geology*, *27*(1), 101–117. https://doi.org/10.1016/j.jsg.2004.06.010

He, D. F., Zhu, W. G., Zhong, H., Ren, T., Bai, Z. J., & Fan, H. P. (2013). Zircon U-Pb geochronology and elemental and Sr-Nd-Hf isotopic geochemistry of the Daocheng granitic pluton from the Yidun arc, SW China. *Journal of Asian Earth Science*, *67-68*, 1–17. https://doi.org/10.1016/j.jseaes.2013.02.002

Hetzel, R., Dunkl, I., Haider, V., Strobl, M., von Eynatten, H., Ding, L., & Frei, D. (2011). Peneplain formation in southern Tibet predates the India-Asia collision and plateau uplift. *Geology*, *39*, 983–986. https://doi.org/10.1130/G32069.1

Horton, B. K., Dupont-Nivet, G., Zhou, J., Waanders, G. L., Butler, R. F., & Wang, J. (2004). Mesozoic-Cenozoic evolution of the Xining-Minhe and Dangchang basins, northeastern Tibetan Plateau: Magnetostratigraphic and biostratigraphic results. *Journal of Geophysical Research*, *109*, B04402. https://doi.org/10.1029/2003JB002913

Horton, B. K., Yin, A., Spurlin, M. S., Zhou, J., & Wang, J. (2002). Paleocene-Eocene syncontractional sedimentation in narrow, lacustrine-dominated basins of east-central Tibet. *Geological Society of America Bulletin*, *114*, 771–786. https://doi.org/10.1130/0016-7606(2002)114<0771

Hou, Z. (1993). Tectonic–magmatic evolution of the Yidun island-arc and geodynamic setting of kuroko-type sulfide deposits in Sanjiang The Region, SW China. In S. Ishihara, T. Urabe & H. Ohmoto (Eds.), *Mineral resources symposia; Volume C. Selected papers from the symposia I-3-47, II-16-5, II-16-10 and II-16-12, ferro-manganese deposits, anoxic sediments and massive sulfide deposits*, *Shigen Chishitsu Special Issue* 17, (pp. 336–350). Tokyo, Japan: Society of Resource Geologists of Japan.

Hu, X., Garzanti, E., Wang, J., Huang, W., An, W., & Webb, A. (2016). The timing of India-Asia collision onset - Facts, theories, controversies. *Earth-Science Reviews*, *160*, 264–299. https://doi.org/10.1016/j.earscirev.2016.07.014

Ingersoll, R. V. (1978). Petrofacies and petrologic evolution of the Late Cretaceous forearc basin, northern and central California. *The Journal of Geology*, *86*(3), 335–352. https://doi.org/10.1086/649695

Ingersoll, R. V., Bullard, T. F., Ford, R. L., Grimm, J. P., Pickle, J. D., & Sares, S. W. (1984). The effect of grain size on detrital modes: A test of the Gazzi-Dickinson point-counting method. *Journal of Sedimentary Petrology*, *54*(1), 103–116. https://doi.org/10.1306/212F83B9-2B24-11D7-8648000102C1865D

Jackson, W., Robinson, D., Weislogel, A., Jian, X., & McKay, M. (2018). Cenozoic development of the nonmarine Mula basin in the southern Yidun terrane: Deposition and deformation in the eastern Tibetan Plateau associated with the India-Asia collision. *Tectonics*, *37*. https://doi.org/10.1002/2018TC004994

Jian, X., Weislogel, A. L., & Pullen, A. (2014). Detrital zircon provenance of the central Songpan-Ganzi turbidites, northern Tibetan Plateau: Implications for the infilling history and tectonic evolution. *Geological Society of America Abstracts with Programs*, *46*(6), 573.

Jian, X., Weislogel, A. L., & Pullen, A. (2015). Detrital zircon U-Pb ages and Hf isotopes of Triassic Songpan-Ganzi and Yidun turbidites and implications for the closure of eastern Paleo-Tethys Ocean. *Geological Society of America Abstracts with Programs*, *47*(7), 38.

Johnston, S., Gehrels, G. E., Valencia, V., & Ruiz, J. (2008). Small-volume U-Pb zircon geochronology by laser ablation-multicollector-ICP-MS. *Chemical Geology*, *259*, 218–229. https://doi.org/10.1016/j.chemgeo.2008.11.004

Kapp, P., DeCelles, P. G., Gehrels, G. E., Heizler, M., & Ding, L. (2007). Geological records of the Lhasa-Qiangtang and Indo-Asian collisions in the Nima area of central Tibet. *Geological Society of America Bulletin*, *119*(7-8), 917–933. https://doi.org/10.1130/B26033.1

Kapp, P., Yin, A., Harrison, T. M., & Ding, L. (2005). Cretaceous-Tertiary shortening, basin development, and volcanism in central Tibet. *Geological Society of America Bulletin*, *117*(7), 865–878. https://doi.org/10.1130/B25595.1

Kapp, P., Yin, A., Manning, C. E., Harrison, T. M., Taylor, M. H., & Ding, L. (2003). Tectonic evolution of the early Mesozoic blueschist-bearing Qiangtang metamorphic belt, central Tibet. *Tectonics*, *22*(5), 1043. https://doi.org/10.1029/2002TC001383

Kidd, W. S. F., Pan, Y., Chang, C., Coward, M. P., Dewey, J. F., Gansser, A., et al. (1988). Geologic mapping of the 1985 Chinese-British Tibetan (Xizang-Qinghai) Plateau geotraverse route. *Philosophical Transactions of the Royal Society of London. Series A*, *327*(1594), 287–305. https://doi.org/10.1098/rsta.1988.0130

Leech, M. L., Singh, S., Jain, A. K., Klemperer, S. L., & Manickavasagam, R. M. (2005). The onset of India-Asia continental collision: Early, steep subduction required by the timing of UHP metamorphism in the western Himalaya. *Earth and Planetary Science Letters*, *234*(1–2), 83–97. https://doi.org/10.1016/j.epsl.2005.02.038

Leng, C. B., Huang, Q. Y., Zhang, X. C., Wang, S. X., Zhong, H., Hu, R. Z., et al. (2014). Petrogenesis of the Late Triassic volcanic rocks in the southern Yidun arc, SW China: Constraints from the geochronology, geochemistry, and Sr-Nd-Pb-Hf isotopes. *Lithos*, *190-191*, 363–382. https://doi.org/10.1016/j.lithos.2013.12.018

Lippert, P. C., van Hinsbergen, D. J. J., & Dupont-Nivet, G. (2014). Early Cretaceous to present latitude of the central proto-Tibetan Plateau: A paleomagnetic synthesis with implications for Cenozoic tectonics, paleogeography, and climate of Asia. *Geological Society of America Special Paper*, *507*, 1–2. https://doi.org/10.1130/2014.2507(01)

Li, W. C., Yu, H. J., Gao, X., Liu, X. L., & Wang, J. H. (2017). Review of Mesozoic multiple magmatism and porphyry Cu–Mo (W) mineralization in the Yidun arc, eastern Tibet Plateau. *Ore Geology Reviews*, *90*, 795–812. https://doi.org/10.1016/j.oregeorev.2017.03.009

Liu, G. (1999). Discovery of Cretaceous palynological Assemblage from the western Sichuan Plateau, SW China and its geological significance. *Acta Micropalaeontologica Sinica*, *16*(1), 54–60. (in Chinese, English abstract).

Liu, Z., Wang, C., & Yi, H. (2001). Evolution and mass accumulations of the Cenozoic Hoh Xil basin, northern Tibet. *Journal of Sedimentary Research*, *71*, 971–984.

Ludwig, K. R. (2012). A geochronological toolkit for Microsoft Excel. *Berkeley Geochronology Center Special Publication*, *5*, 75.

Metcalfe, I. (1996). Gondwanaland dispersion, Asian accretion, and evolution of eastern Tethys. *Australian Journal of Earth Sciences*, *43*(6), 605–623. https://doi.org/10.1080/08120099608728282

Murphy, M. A., Yin, A., Harrison, T. M., Durr, S. B., Chen, Z., Ryerson, F. J., et al. (1997). Did the Indo-Asian collision along create the Tibetan Plateau? *Geology*, *25*(8), 719–722. https://doi.org/10.1130/0091-7613(1997)025<0719:DTIACA>2.3.CO;2

Najman, Y., Appel, E., Boudagher-Fadel, M., Bown, P., Carter, A., Garzanti, E., et al. (2010). Timing of the India-Asia collision: Geological, biostratigraphic, and paleomagnetic constraints *Journal of Geophysical Research*, *115*, B12416. https://doi.org/10.1029/2010JB007673

Nelson, D. R. (2001). An assessment of the determination of depositional ages for Precambrian clastic sedimentary rocks by U-Pb dating of detrital zircon. *Sedimentary Geology*, *141-142*, 37–60. https://doi.org/10.1016/S0037-0738(01)00067-7

Nie, S., Yin, A., Rowley, D. B., & Jin, Y. (1994). Exhumation of the Dabie Shan ultra-high-pressure rocks and accumulation of the Songpan-Ganzi flysch sequence, central China. *Geology*, *22*(11), 999–1002. https://doi.org/10.1130/0091-7613(1994)022<0999:EOTDSU>2.3.CO;2

Orme, D. A., Carrapa, B., & Kapp, P. (2015). Sedimentology, provenance and geochronology of the upper Cretaceous-lower Eocene western Xigaze forearc basin, southern Tibet. *Basin Research*, *27*, 387–411.

Peng, T., Zhao, G., Fan, W., Peng, B., & Mao, Y. (2014). Zircon geochronology and Hf isotopes of Mesozoic intrusive rocks from the Yidun terrane, Eastern Tibetan Plateau: Petrogenesis and their bearings with Cu mineralization. *Journal of Asian Earth Sciences*, *80*, 18–33. https://doi.org/10.1016/j.jseaes.2013.10.028

Pullen, A., Ibanez-Mejia, M., Gehrels, G. E., Ibanez-Mejia, J. C., & Pecha, M. (2014). What happens when *n* = 1000? Creating large-*n* geochronological datasets with LA-ICP-MS for geologic investigations. *Journal of Analytical Atomic Spectrometry*, *29*(6), 971–980. https://doi.org/10.1039/c4ja00024b

Pullen, A., Kapp, P., Gehrels, G. E., Vervoort, J. D., & Ding, L. (2008). Triassic continental subduction in central Tibet and Mediterranean-style closure of the Paleo-Tethys Ocean. *Geology*, *36*(5), 351–354. https://doi.org/10.1130/G24435A.1

Reid, A. J., Wilson, C. J. L., & Liu, S. (2005). Structural evidence for the Permo-Triassic tectonic evolution of the Yidun arc, eastern Tibetan Plateau. *Journal of Structural Geology*, *27*(1), 119–137. https://doi.org/10.1016/j.jsg.2004.06.011

Reid, A. J., Wilson, C. J. L., Liu, S., Pearson, N., & Belousova, E. (2007). Mesozoic plutons of the Yidun arc, SW China: U/Pb geochronology and Hf isotopic signature. *Ore Geology Reviews*, *31*(1-4), 88–106. https://doi.org/10.1016/j.oregeorev.2004.11.003

Robert, A., Zhu, J., Vergne, J., Cattin, R., Chan, L. S., Wittlinger, G., et al. (2010). Crustal structures in the area of the 2008 Sichuan earthquake from geophysics and geology. *Tectonophysics*, *491*(1-4), 205–210. https://doi.org/10.1016/j.tecto.2009.11.010

Roger, F., Jolivet, M., & Malavieille, J. (2010). The tectonic evolution of the Songpan-Garze (North Tibet) and adjacent areas from Proterozoic to present: A synthesis. *Journal of Asian Earth Sciences*, *39*(4), 254–269. https://doi.org/10.1016/j.jseaes.2010.03.008

Roger, F., Malavieille, J., Leloup, P. H., Calassou, S., & Xu, Z. (2004). Timing of granite emplacement and cooling in the Songpan-Garze Fold Belt (eastern Tibetan Plateau) with tectonic implications. *Journal of Asian Earth Sciences*, *22*(5), 465–481. https://doi.org/10.1016/S1367-9120(03)00089-0

Rohrmann, A., Kapp, P., Carrapa, B., Reiners, P. W., Guynn, J., Ding, L., & Heizler, M. (2012). Thermochronologic evidence for plateau formation in central Tibet by 45 Ma. *Geology*, *40*, 187–190. https://doi.org/10.1130/G32530.1

Royden, L. H., Burchfiel, B. C., & van der Hilst, R. D. (2008). The geological evolution of the Tibetan Plateau. *Science*, *321*, 1054–1058.

Rowley, D. B. (1996). Age of initiation of collision between India and Asia: A review of stratigraphic data. *Earth and Planetary Science Letters*, *145*, 1–13.

Shang, F. (2016). Mesozoic History of the southeastern Tibetan Plateau: Sediment provenance, paleoclimate, and surface elevation History, (doctoral dissertation). Retrieved from ProQuest Dissertations Publishing, 2016.10110103. Morgantown, WV: West Virginia University.

Sircombe, K. N. (1999). Tracing provenance through the isotope ages of littoral and sedimentary detrital zircon, eastern Australia. *Sedimentary Geology*, *124*(1-4), 47–67. https://doi.org/10.1016/S0037-0738(98)00120-1

Spurlin, M. S., Yin, A., Horton, B. K., Zhou, J., & Wang, J. (2005). Structural evolution of the Yushu-Nangqian region and its relationship to syn-collisional igneous activity, east-central Tibet. *Geological Society of America Bulletin*, *117*(9), 1293–1317. https://doi.org/10.1130/B25572.1

Studnicki-Gizbert, C., Burchfiel, B. C., Li, Z., & Chen, Z. (2008). Early Tertiary Gonjo basin, eastern Tibet: Sedimentary and structural record of the early history of India-Asia collision. *Geosphere*, *4*(4), 713–735. https://doi.org/10.1130/GES00136.1

Tapponnier, P., Peltzer, G., Le Dain, A. Y., Armijo, R., & Cobbold, P. (1982). Propagating extrusion tectonics in Asia: New insights from simple experiments with plasticine. *Geology*, *10*, 611–616.

Tapponnier, P., Zhiqin, X., Roger, F., Meyer, B., Arnaud, N., Wittlinger, G., & Jingsui, Y. (2001). Oblique stepwise rise and growth of the Tibet Plateau. *Science*, *294*, 1671–1677.

Tian, Y., Kohn, B. P., Gleadow, A. J. W., & Hu, S. (2014). A thermochronological perspective on the morphotectonic evolution of the southeastern Tibetan Plateau. *Journal of Geophysical Research: Solid Earth*, *119*, 676–698. https://doi.org/10.1002/2013JB010429

Vermeesch, P. (2004). How many grains are needed for a provenance study? *Earth and Planetary Science Letters*, *224*(3-4), 441–451. https://doi.org/10.1016/j.epsl.2004.05.037

Vermeesch, P. (2012). On the visualization of detrital age distributions. *Chemical Geology*, *312–313*, 190–194. https://doi.org/10.1016/j.chemgeo.2012.04.021

Wang, B. Q., Wang, W., Chen, W. T., Gao, J. F., Zhao, X. F., Yan, D. P., & Zhou, M. F. (2013). Constraints of detrital zircon U-Pb ages and Hf isotopes on the provenance of the Triassic Yidun group and tectonic evolution of the Yidun terrane, eastern Tibet. *Sedimentary Geology*, *289*, 74–98. https://doi.org/10.1016/j.sedgeo.2013.02.005

Wang, B. Q., Wang, W., & Zhou, M. F. (2013). Provenance and tectonic setting of the Triassic Yidun group, the Yidun Terrrane, Tibet. *Geoscience Frontiers*, *4*(6), 765–777. https://doi.org/10.1016/j.gsf.2013.02.007

Wang, B. Q., Zhou, M. F., Chen, W. T., Gao, J. F., & Yan, D. P. (2013). Petrogenesis and tectonic implications of the Triassic volcanic rocks in the northern Yidun terrane, eastern Tibet. *Lithos*, *175-176*, 285–301. https://doi.org/10.1016/j.lithos.2013.05.013

Wang, B. Q., Zhou, M. F., Li, J. W., & Yan, D. P. (2011). Late Triassic porphyritic intrusions and associated volcanic rocks from the Shangri-La region, Yidun terrane, eastern Tibetan Plateau: Adakitic magmatism and porphyry copper mineralization. *Lithos*, *127*(1-2), 24–38. https://doi.org/10.1016/j.lithos.2011.07.028

Wang, C., Han, W., Wu, J., Lou, H., & Chan, W. W. (2007). Crustal structure beneath the eastern margin of the Tibetan Plateau and its tectonic implications. *Journal of Geophysical Research*, *112*, B07307. https://doi.org/10.1029/2005JB003873

Wang, E., & Burchfiel, B. C. (1997). Interpretation of Cenozoic tectonics in the right-lateral accommodation zone between the Ailao Shan shear zone and the eastern Himalayan syntaxis. *International Geology Review*, *39*(3), 191–219. https://doi.org/10.1080/00206819709465267

Wang, E., & Burchfiel, B. C. (2000). Late Cenozoic to Holocene deformation in southwestern Sichuan and adjacent Yunnan, China, and its role in formation of the southeastern part of the Tibetan Plateau. *Geological Society of America Bulletin*, *112*, 413–423. https://doi.org/10.1130/0016-7606(2000)112<413:LCTHDI>2.0.CO;2

Wang, J. H., Yin, A., Harrison, T. M., Grove, M., Zhang, Y. Q., & Xie, G. H. (2001). A tectonic model for Cenozoic igneous activities in the eastern Indo-Asian collision zone. *Earth and Planetary Science Letters*, *188*, 123–133.

Wang, L., Liu, C., Gao, X., & Zhang, H. (2014). Provenance and paleography of the late cretaceous Mengyejing formation, Simao Basin, southeastern Tibetan Plateau: Whole-rock geochemistry, U-Pb geochronology, and Hf isotopic constraints. *Sedimentary Geology*, *304*, 44–58. https://doi.org/10.1016/j.sedgeo.2014.02.003

Wang, X., Metcalfe, I., Jian, P., He, L., & Wang, C. (2000). The Jinshajiang–Ailoshan suture zone, China: Tectonostratigraphy, age and evolution. *Journal of Asian Earth Sciences*, *18*(6), 675–690. https://doi.org/10.1016/S1367-9120(00)00039-0

Weislogel, A. L. (2008). Tectonostratigraphic and Geochronologic constraints on evolution of the northeast Paleotethys from the Songpan-Ganzi complex, Central China. *Tectonophysics*, *451*(1–4), 331–345. https://doi.org/10.1016/j.tecto.2007.11.053

Weislogel, A. L., Graham, S. A., Chang, E. Z., Wooden, J. L., & Gehrels, G. E. (2010). Detrital zircon provenance from three turbidite depocenters of the Middle-Upper Triassic Songpan-Ganzi complex, central China: Record of collisional tectonics, erosional exhumation, and Sediment Production. *Geological Society of America Bulletin*, *122*(11-12), 2041–2062. https://doi.org/10.1130/B26606.1

Weislogel, A. L., Graham, S. A., Chang, E. Z., Wooden, J. L., Gehrels, G. E., & Yang, H. (2006). Detrital zircon provenance of the Late Triassic Songpan-Ganzi complex: Sedimentary record of collision of the north and south China blocks. *Geology*, *34*(2), 97–100. https://doi.org/10.1130/G21929

Wu, T., Xiao, L., Wilde, S. A., Ma, C. Q., Li, Z. L., Sun, Y., & Zhan, Q. Y. (2016). Zircon U–Pb age and Sr–Nd–Hf isotope geochemistry of the Ganluogou dioritic complex in the northern Triassic Yidun arc belt, eastern Tibetan Plateau: Implications for the closure of the Garzê-Litang Ocean. *Lithos*, *248*, 94–108. https://doi.org/10.1016/j.lithos.2015.12.029

Xiao, L., Zhang, H. F., Clemens, J. D., Wang, Q. W., Kan, Z. Z., Wang, K. M., et al. (2007). Late Triassic granitiods of the eastern margin of the Tibetan Plateau: Geochronology, petrogenesis and implications for tectonic evolution. *Lithos*, *96*(3-4), 436–452. https://doi.org/10.1016/j.lithos.2006.11.011

Xu, L., Rondenay, S., & Van Der Hilst, R. D. (2007). Structure of the crust beneath the southeastern Tibetan Plateau from teleseismic receiver functions. *Physics of the Earth and Planetary Interiors*, *165*(3-4), 176–193. https://doi.org/10.1016/j.pepi.2007.09.002

Yin, A., & Harrison, T. M. (2000). Geologic evolution of the Himalayan–Tibetan orogeny. *Annual Reviews of Earth Planet Science*, *28*(1), 211–280. https://doi.org/10.1146/annurev.earth.28.1.211

Yin, J., Xu, J., Liu, C., & Li, H. (1988). The Tibetan Plateau: Regional stratigraphic context and previous work. *Philosophical Transactions of the Royal Society of London*, *327*, 5–52.

Zahid, K. M., & Barbeau, D. L. Jr. (2011). Constructing sandstone provenance and classification ternary diagrams using an electronic spreadsheet. *Journal of Sedimentary Research*, *81*(9), 702–707. https://doi.org/10.2110/jsr.2011.55

Zhang, K., Zhang, Y., Tang, X., & Xia, B. (2012). Late Mesozoic tectonic evolution and growth of the Tibetan Plateau prior to the Indo-Asian collision. *Earth-Science Reviews*, *114*(3–4), 236–249. https://doi.org/10.1016/j.earscirev.2012.06.001

Zhou, D., & Graham, S. A. (1996). The Songpan-Ganzi complex of the west Qinling Shan as a Triassic remnant ocean basin. In A. Yin & T. M. Harrison (Eds.), *The tectonics of Asia*, (pp. 281–299). Cambridge, UK: Cambridge University Press.